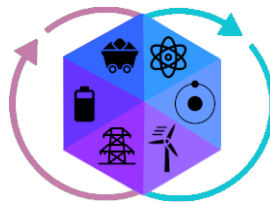


SIMULTANEOUS DESIGN AND OPERATION OF A COAL-FIRED HYBRID ENERGY SYSTEM WITH INTEGRATED THERMAL ENERGY STORAGE

EDNA SORAYA RAWLINGS, NARESH SUSARLA, JAFFER H. GHOUSE, RADHAKRISHNA TUMBALAM GOOTY, ALEXANDER DOWLING, JOHN SIROLA, DAVID C. MILLER



GRID
MODERNIZATION LABORATORY CONSORTIUM
U.S. Department of Energy



DISPATCHES
Design Integration and Synthesis
Platform to Advance Tightly
Coupled Hybrid Energy Systems



November 29, 2023

Disclaimers

This project was funded by the United States Department of Energy, National Energy Technology Laboratory, in part, through a site support contract. Neither the United States Government nor any agency thereof, nor any of their employees, nor the support contractor, nor any of their employees, makes any warranty, express or implied, or assumes any legal liability or responsibility for the accuracy, completeness, or usefulness of any information, apparatus, product, or process disclosed, or represents that its use would not infringe privately owned rights. Reference herein to any specific commercial product, process, or service by trade name, trademark, manufacturer, or otherwise does not necessarily constitute or imply its endorsement, recommendation, or favoring by the United States Government or any agency thereof. The views and opinions of authors expressed herein do not necessarily state or reflect those of the United States Government or any agency thereof.

Sandia National Laboratories is a multimission laboratory managed and operated by National Technology & Engineering Solutions of Sandia, LLC, a wholly owned subsidiary of Honeywell International Inc., for the U.S. Department of Energy's National Nuclear Security Administration under contract DE-NA0003525.

This manuscript has been authored by employees of Lawrence Berkeley National Laboratory under Contract No. DE-AC02-05CH11231 with the U.S. Department of Energy. The U.S. Government retains, and the publisher, by accepting the article for publication, acknowledges, that the U.S. Government retains a non-exclusive, paid-up, irrevocable, world-wide license to publish or reproduce the published form of this manuscript, or allow others to do so, for U.S. Government purposes.

This work was authored in part by the National Renewable Energy Laboratory, operated by Alliance for Sustainable Energy, LLC, for the U.S. Department of Energy (DOE) under Contract No. DE-AC36-08GO28308. Funding provided by U.S. Department of Energy Office of Energy Efficiency and Renewable Energy Solar Energy Technologies Office. The views expressed herein do not necessarily represent the views of the DOE or the U.S. Government.

Edna Soraya Rawlings¹: Conceptualization, Methodology, Software, Formal analysis, Writing - Original Draft, Visualization; **Naresh Susarla**^{2,3}: Conceptualization, Methodology, Software, Validation, Formal analysis, Writing - Original Draft, Visualization; **Jaffer H. Ghose**^{2,3}: Conceptualization, Methodology, Supervision; **Radhakrishna Tumbalam Gooty**^{2,3}: Conceptualization, Writing – Review & Editing; **Alexander Dowling**⁴: Conceptualization, Writing - Review & Editing, Supervision; **John Siirola**⁵: Conceptualization, Writing – Review & Editing, Supervision; **David C. Miller**²: Conceptualization, Writing - Review & Editing, Supervision.

¹Sandia National Laboratories, Livermore, CA

²National Energy Technology Laboratory (NETL), Pittsburgh, PA.

³NETL support contractor, Pittsburgh, PA.

⁴Department of Chemical and Biomolecular Engineering, University of Notre Dame, Notre Dame, IN.

⁵Sandia National Laboratories, Albuquerque, NM.

*Corresponding contact: d.c.miller.phd@gmail.com

Acknowledgements:

This work was conducted as part of the Design Integration and Synthesis Platform to Advance Tightly Coupled Hybrid Energy Systems (DISPATCHES) project through the Grid Modernization Lab Consortium with funding from the U.S. Department of Energy's Office of Fossil Energy and Carbon Management, Office of Nuclear Energy, and Hydrogen and Fuel Cell Technology Office.

Suggested Citation:

E.S. Rawlings, N. Susarla, J.H. Ghose, R. Tumbalam Gooty, A. Dowling, J. Siirola, and D.C. Miller, "Simultaneous Design and Operation of a Coal-fired Hybrid Energy System with Integrated Thermal Energy Storage", National Energy Technology Laboratory, Pittsburgh, November 29, 2023.

DISPATCHES TEAM

National Energy Technology Laboratory

David Miller, Jaffer Ghouse^{1,2}, Andrew Lee¹, Radhakrishna Tumbalam Gooty¹, Naresh Susarla^{1,2}, Andres Joaquin Calderon Vergara^{1,2}

Sandia National Laboratories

John Siirola, Darryl Melander, Edna Soraya Rawlings, Kyle Skolfield, Jordan Jalving²

Lawrence Berkeley National Laboratory

Dan Gunter, Oluwamayowa Amusat, Keith Beattie, Ludovico Bianchi

National Renewable Energy Laboratory

Wesley Jones, Darice Guittet, Benard Knueven, Ignas Satkauskas, Abinet Eseye²

Idaho National Laboratory

Aaron Epiney, Joshua Cogliati, Andrea Alfonsi², Konor Frick², Jason Hansen, Cristian Rabiti², Jakub Toman, Elizabeth K. Worsham, Ramon K. Yoshiura, Gabriel J. Soto Gonzalez, Richa K. Sabharwall

University of Notre Dame

Alexander Dowling, Xinhe Chen, Xian Gao²

¹NETL Support Contractor

²Contributed to the project but the person is no longer affiliated with the organization.

Executive Summary

The introduction of renewable energy to the grid is forcing traditional thermal generators that were originally designed for base-load operations, such as coal-fired and natural gas combined cycle (NGCC) power plants, to undergo frequent load ramping. The integration of thermal energy storage systems (TES) to base-load thermal generators offers an opportunity to increase the flexibility of these generators since it allows them to store energy (charge) at unfavorable times, such as periods of low demand or low electricity prices, and use this stored energy (discharge) at more favorable times, such as during periods of high demand or high electricity prices, to generate additional power.

The integration and design of TES for the flexible operation of thermal generators in the context of dynamic energy markets involves at least two key challenges. The first is to determine the best locations for adding and removing heat from the plant. This process-level integration of the storage involves evaluating multiple discrete decisions for the selection of storage materials and process streams for heat transfer from within the power plant to charge and discharge the TES. These discrete choices introduce combinatorial complexity to the inherently nonlinear process operations. Existing approaches address this issue by limiting the number of choices to explore since the evaluation of the integration of the TES system involves the construction of multiple models, one for each design, restricting their design search space. The second key challenge is the optimal sizing of the TES system in dynamic electricity markets, which has been largely ignored in the analysis of thermal generators since electricity prices have historically been assumed to be time-invariant, leading to either over-sizing or under-sizing the required TES.

In this work, we present a generalized combinatorial dynamic optimization approach to address these two challenges for the design and integration of a molten salt-based TES with an ultra-supercritical power plant (USCPP). To demonstrate the proposed approach, we built first-principle process models, including rigorous property calculations and dynamic electricity prices for designing a TES. For modeling and analysis, we use the open-source tools and methods developed under the Design Integration and Synthesis Platform to Advance Tightly Coupled Hybrid Energy Systems (DISPATCHES) project, which leverages the IDAES[®] modeling platform. To keep the problem computationally tractable, the proposed approach consists of two steps:

Step 1. Implementation of a Generalized Disjunctive Programming (GDP) formulation for the design and integration of a TES with the USCPP. We built two GDP superstructures, one to charge and one to discharge the TES, to determine the optimal points for their integration with the USCPP.

Step 2. Formulation of a multi-period optimization problem for the integrated USCPP considering the optimal discrete choices obtained in Step 1. In this multi-period model, we use time-varying electricity prices for an average day and week of the year based on the Reliability Test System's (RTS-GMLC) open-source data set under a price-taker assumption.

The results from the two-step approach lead to new integrated processes and system-level insights for hybrid USCPP energy systems. Using an optimization-based technique, we identified multiple feasible designs to integrate a thermal TES with the USCPP. This analysis helps determine the relative impacts of different discrete design decisions on the overall cost. The TES design obtained from considering time-varying electricity prices lowered the capital costs by 40% and had higher utilization of 89% (vs. 32%) as compared to the design obtained from the traditional approach of using time-invariant electricity prices during design. Finally, we observed an 18% increase in profit when the design problem is solved considering electricity prices for an entire week as compared to a day, which highlights the need for considering longer time horizons when designing TES for monthly or seasonal storage.

The general framework proposed in this work is a design approach that can be easily applied to explore other hybrid or integrated thermal energy systems such as NGCC with CO₂ capture, biomass gasification for co-producing hydrogen and electricity with CO₂ capture, nuclear power generators with TES, and concentrated solar power (CSP) with TES. Finally, the outlined integrated energy systems can also be evaluated in a specific electricity market by using historical electricity prices instead of the RTS-GMLC dataset used in this study.

Contents

1	Introduction and Literature Review	8
1.1	Dynamic Energy Markets Drive Economics of Integrated Energy Systems	8
1.2	Thermal Energy Storage Increases Flexibility of Integrated Energy Systems	9
1.3	Importance of Optimization for Integrated Energy Systems and Thermal Energy Storage	10
1.4	Novel Contributions	11
1.5	Report Organization	11
2	Methods	12
2.1	Problem Statement	12
2.2	Time-varying Electricity Prices	13
2.3	Ultra-supercritical Power Plant (USCPP)	14
2.4	Optimization Formulation	16
3	Results	26
3.1	Step 1: Generalized Disjunctive Programming Design	26
3.2	Step 2: Multi-period Optimization Under Price-taker Assumption	30
4	Conclusions	34
A	Ultra-supercritical Power Plant and Storage System Models	36
B	Data for Ultra-supercritical Power Plant Model	37

C Average RTS-GMLC Data	38
D GDP Superstructures Feasible Designs	40

List of Tables

1	Problem statement of multi-period optimization problem	12
2	Discrete design decisions in charge and discharge GDP superstructures.	18
3	Description of design decisions as disjunctions in charge GDP superstructure.	20
4	Description of design decisions as disjunctions in discharge GDP superstructure.	20
5	Results for the discrete and continuous design decisions for the top seven feasible designs and the last feasible design for the charge GDP superstructure of the ultra-supercritical power plant.	26
6	Results for the discrete and continuous design decisions for the top seven and last feasible designs for the discharge GDP superstructure for the ultra-supercritical power plant. The variables marked with an * are variables that have a fixed value during the optimization.	28
7	Results for the operation-only and simultaneous design and operation of the integrated ultra-supercritical power plant for the average-day and average-week. The variables marked with an * are variables that have a fixed value during the optimization.	31
8	Results for the individual days in the average-week time horizon for the simultaneous case multi-period model.	33
9	IDAES [®] unit models used for the construction of the ultra-supercritical power plant model.	36
10	DISPATCHES and IDAES [®] property packages used in the ultra-supercritical power plant model integrated with storage system.	36
11	Data for the ultra-supercritical power plant model.	37

List of Figures

1	Histogram of RTS-GMLC data set for one year. The inset at the top right shows the frequency for electricity prices π above \$40 per MWh.	14
2	Process flow diagram for the ultra-supercritical plant.	15
3	TES units for (a) charge and (b) discharge processes.	16
4	Process flowsheet for the (a) charge and (b) discharge GDP superstructures of the ultra-supercritical plant. The flowsheets include colored dashed lines that represent the design alternatives for each design decision or disjunction. In (a) or charge superstructure, the disjunction 1 and its alternatives are shown as green dashed lines, disjunction 2 as red dashed lines, disjunction 3 as blue dashed lines, and disjunction 4 as yellow dashed lines. In (b) or discharge superstructure, the disjunction 1 and its eleven alternatives are shown as the blue dashed lines.	19
5	Step 2 or multi-period step approach for the simultaneous design and operation of the integrated ultra-supercritical power plant.	25
6	Optimal process flowsheet for ultra-supercritical plant (USCPP) integrated with (a) charge and (b) discharge TES after the solution of the GDP superstructures in Step 1.	29
7	Process flowsheet of optimal integrated ultra-supercritical power plant with charge and discharge cycles at the optimal points of integration found during GDP design Step 1.	30
8	Optimal profiles for the hot and cold salt amount for the (a) operation-only average-day, (b) operation-only average-week, (c) simultaneous design and operation for the average-day, and (d) simultaneous design and operation for the average-week.	33
9	RTS-GMLC dataset for the average-day and average-week of the year.	39
10	Results for the (a) profit (a) and (b) area of charge heat exchanger for all feasible designs identified during the solution of the discrete design decisions of the charge USCPP superstructure. The feasible designs correspond to 55 of the 60 explored configurations.	41

11	Results for the (a) profit and (b) area of discharge heat exchanger for all feasible designs identified during the solution of the discrete design decisions of the discharge USCPP superstructure.	42
----	---	----

1. Introduction and Literature Review

1.1 Dynamic Energy Markets Drive Economics of Integrated Energy Systems

The introduction of renewable energy sources to the power grid has caused a reduction in the energy produced by base-load power plants such as coal-fired and nuclear plants that have been traditionally considered the main dispatchable units in the grid [1]. To facilitate expansion of variable renewable generation sources into the grid, base-load power plants undergo frequent increases and reductions in power generation, highlighting one of their main limitations: the low speed and inefficiency with which the generators can increase (ramp-up) or decrease (ramp-down) power generation. In thermal power plants, this variable generation and frequent shut-downs and start-ups increase thermal stress on various components of the plant equipment, such as boiler and steam turbines, reducing their life and performance and increasing their maintenance and replacement costs [22, 28].

One approach to make dispatchable plants more resilient and flexible is to integrate them with thermal energy storage systems (TES) to create an integrated energy system (IES) that combines a power generator with energy storage to provide an additional thermal reserve [27]. The integration of energy storage systems with power plants not only increases the flexibility of the generator but also enables the plant to operate closer to base load. In modern electricity grids, IES can provide flexibility to offset uncertainty from renewables and new energy demands while also helping to address ramping concerns [17]. However, their design is an inherently challenging problem since it involves not only multiple discrete design decisions related to the integration of TES with the power plant, such as alternative integration points, storage materials to use, and size of the storage, but also determining operating conditions. These design decisions are critical for determining how fast the generator can ramp, which impacts how the generator can bid into the electricity market. Hence, to accurately design an IES that can realistically operate in a current electricity market, we need to analyze how rapidly these systems can respond to changes in the market and how they impact market revenue. A popular approach to maximize the economic benefits of an IES is to consider historical or synthetic dynamic prices of electricity while neglecting the impact of the IES bids on the market [12]. This approach, referred to as the *price-taker* approach, has previously been adopted for the study of integrated concentrated solar plants, where it has shown its usefulness for the design and optimization of more flexible concentrated solar power (CSP) systems [33, 29, 13].

1.2 Thermal Energy Storage Increases Flexibility of Integrated Energy Systems

Thermal energy storage systems store and release sensible or latent heat by heating and cooling a storage material. Some of the most popular storage materials are water, thermal oils, and molten salts due to their low cost and favorable thermo-physical properties such as high boiling point and thermal stability. Alva et al. [2] and Sun et al. [35] present an overview of different TES, their advantages, and the systems into which they have been integrated. In a sensible heat-based TES, the storage material undergoes two different operations: charging, where the storage material is heated and stored in an insulated tank, and discharging, where the energy from the previously stored hot storage material is extracted and integrated with the IES.

Many studies in the literature have explored the importance of the integration of TES and how it can improve the performance of existing thermal generators. Yet most of these studies rely on simulation models under the assumption that either the points of integration of the TES with the energy system are known or that other design variables such as storage material and storage heat capacity and size, etc., are known and given *a priori*. For example, Garbrecht et al. [18] and Li and Wang [27] solved simulation models to study multiple strategies to integrate molten salt-based TES with coal-fired thermal power plants with the objective of evaluating the power plant operating range while reducing fluctuations of the power grid. Yong et al. [41] proposed simulation models for the integration of a TES in a coal-fired supercritical power plant with the objective of replacing the boiler in the process, showing that the integrated plant has a higher thermal efficiency than the original plant (41.8% compared to 40.3%, respectively). Other studies considered different types of TES systems and their effect in coal-fired power plants. For example, Krugger et al. [25] evaluated multiple TES systems (molten salt-based, solid media storage, and a Ruth's type steam accumulator) with a coal-fired power plant to perform a comparative evaluation of these different TES technologies and determined that each system has different net capacity during load increase (or discharging) and load reduction (charging) of the power plant and TES efficiencies. However, a commonality among these simulation studies is that the TES system is integrated with coal-fired power plants assuming a fixed connection to the power plant cycle without considering other connection points.

To determine the effect that different steam sources have on the performance of the IES, Wojcik and Wang [38] performed a study that exhaustively simulated multiple options to determine the best point source of steam in a subcritical conventional oil-fired power plant for extracting heat through a heat exchanger (with no specific TES technology), where the outlet conditions for the steam were fixed *a priori*. Zhang et al. [42] also presented a simulation model to evaluate the performance of a molten salt-based TES system when using high-temperature flue gas and superheated steam sources in an integrated coal-fired power plant, where they found that the round-trip efficiency of the TES system is up to 85.17% when using the appropriate match between the heat sources and the TES media. However, even when these studies show clear benefits of integration of TES with coal-fired power plants while exploring the effect of multiple heat sources in IES, the points of steam extraction, storage material, and TES technology were known and fixed during the solution of the model, resulting in the exploration of only a small set of possible design alternatives, which can lead to a sub-optimal design of the IES.

1.3 Importance of Optimization for Integrated Energy Systems and Thermal Energy Storage

In contrast to the approaches described above, optimization-based approaches provide a systematic framework to determine how to best integrate TES technologies with power plants. Specifically, Yeomans and Grossmann [39], Mencarelli et al. [30], and Chen et al. [10] proposed a strategy that requires the construction of a superstructure. A superstructure includes possible alternative interconnections of technologies. The superstructure model then contains the equations and connections of all the possible technologies, their interconnections, and their operational constraints. This approach, known as superstructure optimization, is used to select the optimal structure from many alternatives within a single optimization problem.

Superstructure optimization aims to provide a systematic approach to explore a large design space. To achieve this, we need to first accurately postulate all relevant configurations of the process alternatives and their interconnections, followed by the formulation of the mathematical programming model. The solution of this model identifies the optimal structure. The translation from superstructure to a mathematical model can be done using various optimization techniques, such as mixed-integer nonlinear programming (MINLP) or Generalized Disjunctive Programming (GDP). MINLP has been extensively used to solve conceptual design problems in which continuous and discrete (0-1) variables are introduced to the problem to model the discrete choices in a process superstructure [36]. Applied to energy systems, for example, Fuentes-Cortés et al. [16] proposed a MINLP superstructure approach to determine multiple design decisions in a cooling, heating, and power production system, including sizing and selection of prime mover and sizing of the TES and auxiliary thermal system. Applied to the study of IES, Dowling et al. [13] implemented a MINLP formulation in a decomposition algorithm to perform simultaneous scheduling and control decisions in an integrated CSP system, where they quantify the revenue potential of the concentrated solar system while also exploring the effects of the design variables on revenue potential. Despite their successful application, MINLP formulations are challenging to solve, especially for complex energy systems that include nonlinear equations.

GDP is a more intuitive approach for the conceptual design of prospective technology alternatives, which introduces disjunctions, Boolean variables, and logic propositions to the optimization problem to represent discrete design decisions. These disjunctions, written following a natural syntax that groups sets of constraints to every alternative within each discrete decision, have a logical structure that is exploited to avoid zero-flow streams that affect the numerical solution when streams or connections disappear. GDP has been used for the conceptual design of chemical and energy processes, where its implementation allowed the systematic evaluation of a broad range of design decision parameters [40, 23, 5, 4, 24]. In these studies, a design model is constructed for each specific case study using an equation-oriented algebraic modeling language in which the modeler explicitly included all the equations involved in their system and the reformulations of the logic-based equations and discrete variables involved in the GDP formulation. To fully benefit from GDP modeling, the tool `Pyomo.GDP` [9] was developed to easily perform the reformulations and other model transformations needed in a GDP problem formulation, while also allowing the implementation of advanced mathematical algorithms for their solution. In recent studies, Chen et al. [10], Rawlings et al. [31], and Ghouse et al. [19] illustrate the use of this modeling tool for the synthesis and conceptual design of complex processes, such as the synthesis of a flowsheet of eight potential process units, a methanol synthesis process with multiple alternatives for feed

and reactor units, and multi-product distillation columns. In these studies, multiple design decisions are included in each GDP model and are simultaneously calculated without the need for any reformulations from the modeler. Nevertheless, its use for the conceptual design of IES is still limited. One reason is the lack of process simulation tools that support not just an equation-oriented and user-friendly environment with greater flexibility for the construction of complex power plant flowsheets and design models that can represent real-world power generation systems, but also the capability to link advanced algorithms that can support the automatic reformulation of GDP logical relations.

1.4 Novel Contributions

To address the aforementioned challenges, we use DISPATCHES (Design Integration and Synthesis Platform to Advance Tightly Coupled Hybrid Energy Systems), an open-source platform built on IDAES[®] [26] for the optimization and design of hybrid energy systems. In this study, we leverage its capabilities for the construction of first-principle rigorous models and superstructures to perform the analysis and optimization of a pulverized coal-fired ultra-supercritical power plant (USCPP) that is integrated with a TES. We also make use of open-source grid-integration tools to study the effect of electricity prices on the design of a TES by solving a multi-period simultaneous design and optimization problem. This study aims to advance the state of the modeling and conceptual design of IES and quantify their potential impact using open-source platforms and cutting-edge design optimization formulations in a multi-period approach. This work makes three novel contributions to the design and operation of integrated energy systems:

1. We propose and systematically evaluate multiple design configurations of an integrated thermal energy system with a monolithic model using GDP, a logic-based optimization approach.
2. We explore the use of open-source platforms DISPATCHES and IDAES[®] to construct first-principle rigorous models for complex energy systems, with the flexibility to connect and disconnect streams in the flowsheet, to explore multiple configurations.
3. We determine the influence of the electricity market on the optimal design and operation of IES. Toward this, we develop a two-step optimization approach to determine the optimal size and market participation of energy systems with TES that maximize the profit.

1.5 Report Organization

The remainder of this report is organized as follows: Section 2 describes all the methods used in this study, including Section 2.1 that states the multi-period optimization problem under the price-taker assumption; Section 2.2 defines the electricity market data used during the multi-period model under the price-taker assumption; Section 2.3 describes the model for the USCPP and storage systems; and Section 2.4 describes the mathematical formulations of the optimization problems for the design and simultaneous design and operation of the integrated USCPP system. Section 3 presents results and discussion, and the report culminates in Section 4, where we draw conclusions of the analyses, present the major contributions of the work, and outline future research.

2. Methods

2.1 Problem Statement

The primary objective of this work is to optimally design and integrate a TES with a USCPP while considering the impact of time-varying electricity prices. We propose a multi-period optimization problem under the price-taker assumption for the simultaneous design and operation of an integrated energy system. The problem is summarized in Table 1.

Table 1: Problem statement of multi-period optimization problem

Given:	Ultra-supercritical power plant model Operational conditions of the power plant flowsheet Time series electricity prices
Determine:	(a) Points of integration of TES with power plant during charge and discharge processes (b) Storage material in TES (c) Size of storage heat exchangers in TES (d) Temperature of storage material in TES (e) Schedule of TES system
Objective:	Maximize a net profit function
Subject to:	Mass and energy balances Power plant and TES performance equations Ramping constraints Storage material mass balances Non-anticipativity constraints

In this optimization problem, we consider two types of design decisions:

1. Discrete design decisions (d^d) include items (a) and (b) in Table 1, such as determining where to integrate the charge and discharge connections within the power plant and selecting the storage materials. The points of integration of TES with the power plant are selected considering the conditions needed for the charge and discharge processes, while three different storage materials are considered: Solar salt, Hitec salt, and thermal oil.
2. Continuous design decisions (d^c) include the variables in (c) and (d) in Table 1, such as the size of the TES heat exchangers and temperature of the storage material. When determining

these decisions, we simultaneously solve for the schedule (e) of the TES, i.e., the mode of operation (charge or discharge) as a function of the time-varying electricity prices.

All the models constructed for the USCPP and the integrated USCPP, including the superstructures for the conceptual design of the USCPP integrated with charge and discharge processes, are included as part of the open-source DISPATCHES model library available at <https://github.com/gmlc-dispatches/dispatches>. They are constructed using the open-source platforms DISPATCHES (version 1.3.0), IDAES[®] [26] (version 2.0.0), and Pyomo [7] (version 6.5.0). Since IDAES[®] uses Pyomo as its core modeling framework, we gain access to a flexible set of automatic reformulation and solution algorithms from which we can select the best tool to optimize the proposed models and superstructures. To determine the discrete design decisions, we use Pyomo GDPopt [9] (version 22.5.13) since it provides an automatic reformulation of the logical constraints to their algebraic form without any further reformulations from the user. For GDPopt, we use Gurobi [21] (version 10.0.1) as the linear solver and IPOPT [37] (version 3.13.2) as the local/nonlinear solver. To determine the continuous design decisions and TES schedule, we use the solver IPOPT (version 3.13.2). All the analyses reported in this study were performed on a Dell Precision 5560 laptop with 11th Gen Intel(R) Core(TM) i9-11950H @ 2.60GHz, having 32.0 GB RAM, and running Windows 11 Pro. The remainder of this section describes the time-varying electricity prices (Section 2.2), USCPP and TES mathematical models (Section 2.3), and the decomposition strategy for the optimal design and operation of the integrated power plant (Section 2.4).

2.2 Time-varying Electricity Prices

The Reliability Test System (RTS) is a collection of synthetic grids that assist the engineering community in understanding how new technologies and operational practices might impact the power system cost and performance of the grid. As part of the United States Department of Energy’s Grid Modernization Initiative, Barrows et al. [3] implemented a variety of updates to the RTS-96 generation and load data [20] to modernize the power generation sources and their geographic and temporal variability. The updated grid, known as the RTS-GMLC, has 73 buses distributed in three regions with 120 transmission lines. It consists of 73 thermal generators (coal, oil, and natural gas generators), one nuclear generator, 81 renewable generators (hydro, utility-scale photo-voltaic, and rooftop photo-voltaic), and one storage unit. Of the thermal generators in the modernized grid, only 16 use coal. The RTS-GMLC dataset includes time series for year-long simulations of hourly 24-hour ahead forecasts and is available at <https://github.com/GridMod/RTS-GMLC>. The dataset used in this study contains a total of $364 \text{ days} \times 24 \text{ hours} = 8,736$ time values of the locational marginal price (LMP) (denoted as π hereafter). The dataset contains π values ranging between \$0 and \$200 per MWh. Figure 1 shows the histogram or the frequency distribution of the dataset for one year. The inset at the top right of the figure shows the frequency for π values above \$40 per MWh. Figure 1 shows that about 20% of the data have values between \$0 and \$10 per MWh (the majority having been zero values), 14% of the data between \$10 and \$20 per MWh, and 65% of the data between \$20 and \$40 per MWh. The remaining 1% of the data have values higher than \$40 per MWh.

To study the effect of the electricity market on the optimal design and operation of the USCPP integrated with a TES, we calculate the average price of electricity for one representative day and one representative week of the year considering the π at each hour of the day and week for the

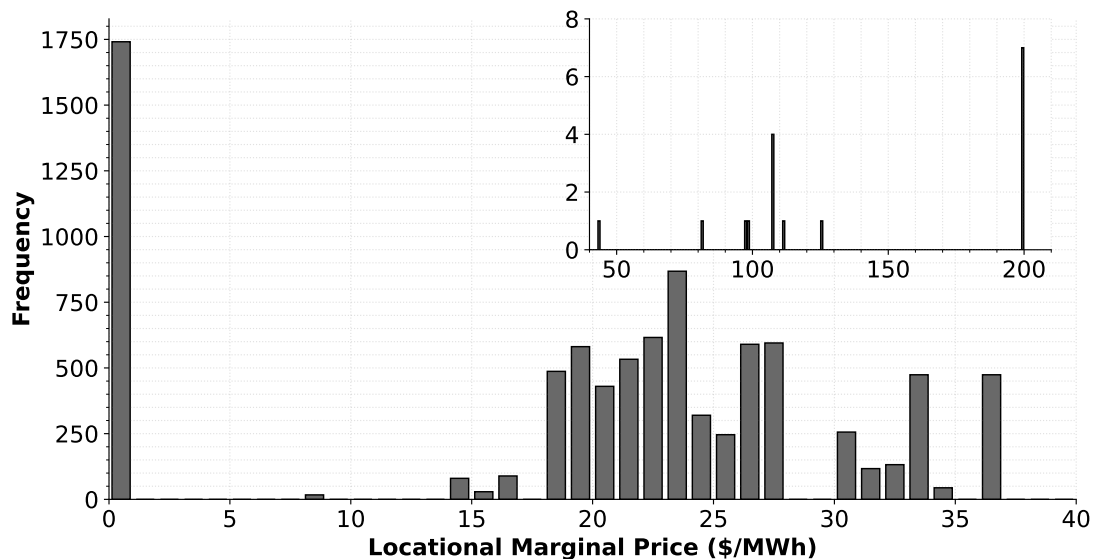


Figure 1: Histogram of RTS-GMLC data set for one year. The inset at the top right shows the frequency for electricity prices π above \$40 per MWh.

364 days of the year. In future sections, we refer to these time horizons as an *average-day* (24-hour time period) and an *average-week* (168-hour time period). Appendix C includes Figures 9a and 9b, which show the calculated average data for the average day and average week from the RTS-GMLC data, respectively. These average values are used to determine the hourly schedule of TES and the operation of the integrated USCPP.

2.3 Ultra-supercritical Power Plant (USCPP)

Integrated coal-fired power plants involve the connection of an energy storage system to the main thermal cycle of the thermal generator. To construct an integrated power plant model, we first define the type of coal-fired thermal generator to use, followed by the construction of a rigorous model that can accurately describe its behavior. In this study, we consider a pulverized coal-fired ultra-supercritical power plant based on a 400 MWe single unit given in Department of Energy technical report DOE/FE-0400 [11]. To construct the integrated power plant, we propose the integration of a TES system that is connected to the main thermal cycle in the plant to increase the base-load plant flexibility during energy production.

The USCPP is similar to the supercritical power generation units, but it operates at even higher temperatures and pressures (above 600 °C with steam pressures ranging from 25 to 29 MPa) enabling the employment of a more efficient steam cycle that can reduce fuel consumption and CO₂ emissions when compared to subcritical and supercritical generators [6]. The steam cycle in the USCPP is based on a double reheat configuration with a sequence of turbines (Turb) operating from very high pressure (VHP) to low pressure (LP) (2.60 to 31.12 MPa). The reheaters Reheat₁ and Reheat₂ are used to reheat the exhaust steam from the VHP turbines 1 and 2 (Turb₁ and Turb₂) and the

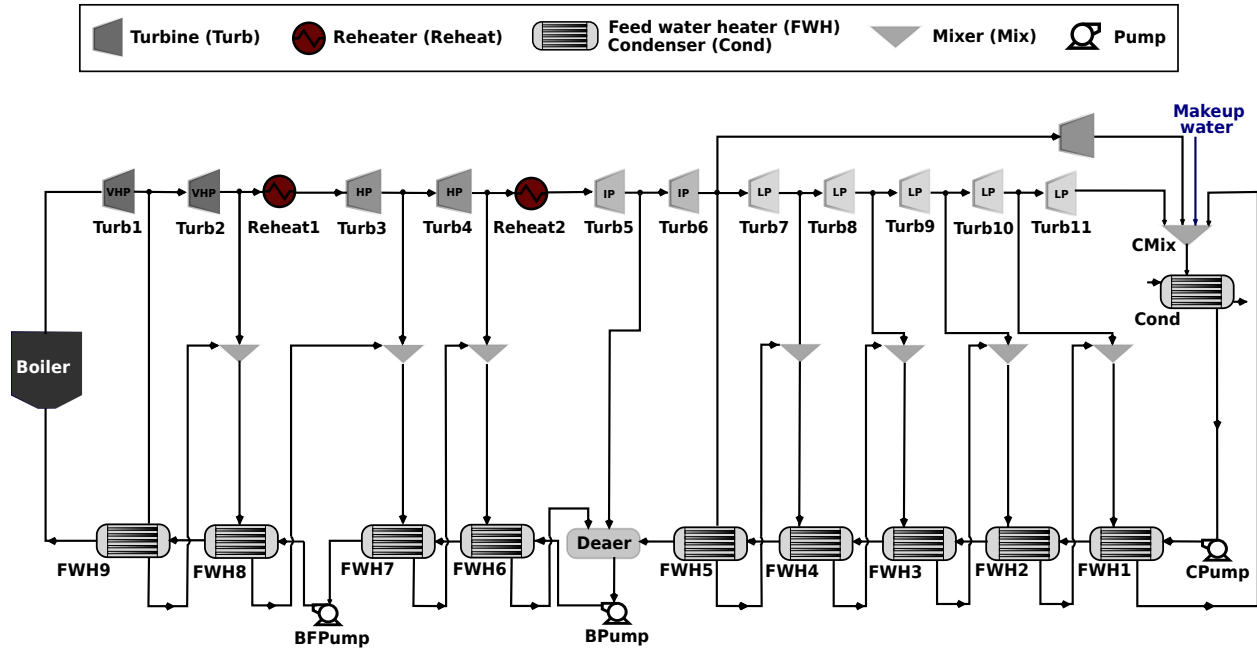


Figure 2: Process flow diagram for the ultra-supercritical plant.

high pressure (HP) turbines 3 and 4 (Turb₃ and Turb₄) before it enters the intermediate pressure (IP) turbine 5 (Turb₅). Figure 2 shows a process flowsheet of the USCPP. The last LP turbine 11 (Turb₁₁) exhausts to a single pressure condenser. The feed water train consists of nine closed feed water heaters (FWH) of which five operate at low pressure (FWH₁ to FWH₅), four at high pressure (FWH₆ to FWH₉), and one open feed water heater or deaerator (Deaer). A condensate is pumped to the deaerator inlet from the outlet of the low-pressure feed water train (FWH₅). Feed water from the deaerator is then pumped to the boiler inlet. Extractions for feed water heating, deaerating, and as an inlet for the boiler feed pump (BFPump) are taken from the high, intermediate, and lower pressure turbine cylinders and from the cold reheater. The plant is designed to be operated as a base-load unit since the cycle is best suited operationally for this type of dispatch mode.

To construct the first-principle rigorous model for the USCPP, we use DISPATCHES and IDAES[®] [26] open-source platforms, which contain a library of customizable unit models for heat exchangers, turbines, and thermophysical properties of water as the working fluid in the thermal cycle. IDAES[®] unit models contain the energy and mass conservation equations needed in the power system, while the working fluid property package includes properties such as density, viscosity, enthalpy, etc. Appendix A includes all the details about the unit models and their process assumptions and the used property packages for the construction of the USCPP and TES system models. Appendix B shows the process flowsheet data, design parameters, and operational conditions for the USCPP. All the units in the USCPP flowsheet are connected using the modeling component Arcs from Pyomo, and once linked, all the units are initialized by propagating the state variables through the connected ports using the IDAES[®] propagate_state initialization procedure. More details about this procedure can be found in the IDAES[®] documentation. Once built, this USCPP model is used as the base model to construct design superstructures and the integrated USCPP model.

Thermal Storage System

A TES system integrates a charge and a discharge process with an energy system to store sensible heat and produce steam with the stored energy. For this thermal exchange to occur, each process in the TES requires the use of a heat exchanger to transfer heat between a hot and cold source and the storage material and auxiliary units to return the working fluid to the plant cycle. Figure 3a shows the charge process that includes a heat exchanger (HX), a storage pump (SPump) to ensure that the condensed steam is at the right pressure before recycling it back to the power plant, and an insulated tank to store the hot storage material. Figure 3b shows a typical discharge process that includes a heat exchanger, a storage turbine (STurb) to produce power with the newly generated steam, and a tank to store the cold storage material. These models are constructed using the IDAES[®] countercurrent heat exchangers with log mean temperature differences for both heat exchangers, while the other unit models and property packages for storage materials are given in Appendix A.

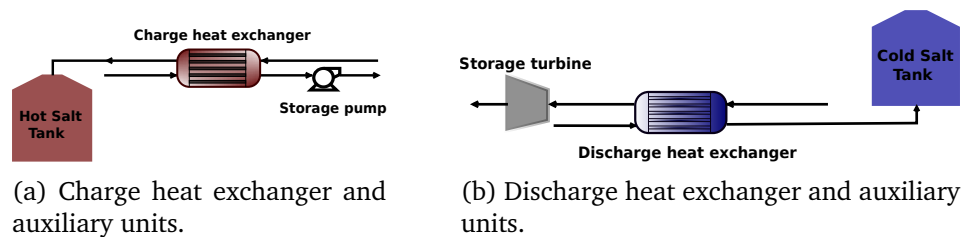


Figure 3: TES units for (a) charge and (b) discharge processes.

The construction of more flexible, economically viable integrated power plants requires the integration of TES processes with energy systems, but their connection requires the definition of various discrete design decisions. One decision is the selection of the storage material to use in the TES, since the amount of thermal energy that is stored depends on the heat capacity and temperature range of the material. It is also important to consider the operational conditions of the heat transfer fluid, such as temperature and pressure, which are controlled by the point where the heat transfer fluid is extracted from an energy system. In an IES, these conditions are dictated by the point of integration of the charge and discharge processes within the thermal cycle. Consequently, to integrate a TES with the USCPP, we need to select a storage material that enhances the capabilities of the plant and a working fluid from the main thermal cycle in the plant that can exploit the heat capacity of the storage material so that when integrated, the hybrid USCPP can respond to the power requirement from the grid.

2.4 Optimization Formulation

For the simultaneous design and operation of the integrated USCPP problem given in Section 2.1, we propose a two-step approach to determine all design and operational variables in items (a) to (e) in Table 1. These steps are described below:

1. GDP: Calculate the discrete design decisions d^d in (a) and (b) in Table 1, i.e., the storage material and the optimal points of integration of the TES system for charge and discharge processes, using a GDP formulation.

2. Multi-period: Calculate the continuous design decisions d^c in (c) and (d) in Table 1 to determine the size and operational conditions of the USCPP and TES when considering the electricity market. To determine these design variables, we implement the integrated model of an USCPP (constructed using the discrete design decisions found in Step 1) in a multi-period model under a set of fixed electricity prices. With the solution of this multi-period optimization problem, we simultaneously determine the remaining item (e).

To maximize the economic benefits of the IES in Step 2, we consider the price of electricity, neglecting how the energy system bids impact the market. This price-taker problem optimizes the dispatch of energy systems against RTS-GMLC electricity prices to maximize the revenue of the energy system. This is done during the solution of the problem, where the highest dispatch of the energy system coincides with periods of high electricity prices. In this study, we intend to demonstrate that by considering the design and operational problems separately in the analysis of energy systems, we could be operating integrated energy systems with under-designed or over-designed TES. This can result in unnecessary increments in capital and operating costs during the operation of the integrated power plant, which can turn these hybrid systems into undesirable alternatives in real energy production processes.

Step 1: Superstructure Design Using Generalized Disjunctive Programming

To ensure the exploration of multiple alternative configurations within the same model, we propose a GDP optimization strategy to systematically explore 71 possible configurations arising from the discrete design decisions in Table 2. To build the two superstructures, one for charging and one for discharging, we disconnect multiple streams from the USCPP flowsheet in Figure 2 to open alternatives to connect the charge and discharge heat exchangers and their auxiliary units (Section 2.3). Once we have alternative points to connect the TES in the USCPP, we construct the GDP design superstructure models in Figure 4, in which the discrete design decisions are formulated as disjunctions following the discrete design decisions for each storage process in Table 2. For the proposed charge GDP superstructure in Figure 4a, where the TES heat exchanger stores energy in a storage material and then recycles condensed steam back to the plant, we consider four disjunctions: (1) selection of a storage material (green dashed lines), (2) selection of a steam source to heat the storage material (red dashed lines), (3) selection of a connection point within the plant for the return of the condensed steam back to the power plant (blue dashed lines), and (4) selection of a cooler after the charge storage process to enforce that the condensed steam is at the right pressure before recycling it back to the plant (yellow dashed lines). Note that in Figure 4a in the dashed blue lines for disjunction 3, a recycle mixer 5 (RMix₅) is included to mix the outlet from the charge storage process with the condensed steam coming from the feed water train alternatives. Only the representation of one recycle mixer RMix is included to avoid saturating the flowsheet, but the names of the other recycle mixers for each alternative are included with a black circle (RMix₁ to RMix₄).

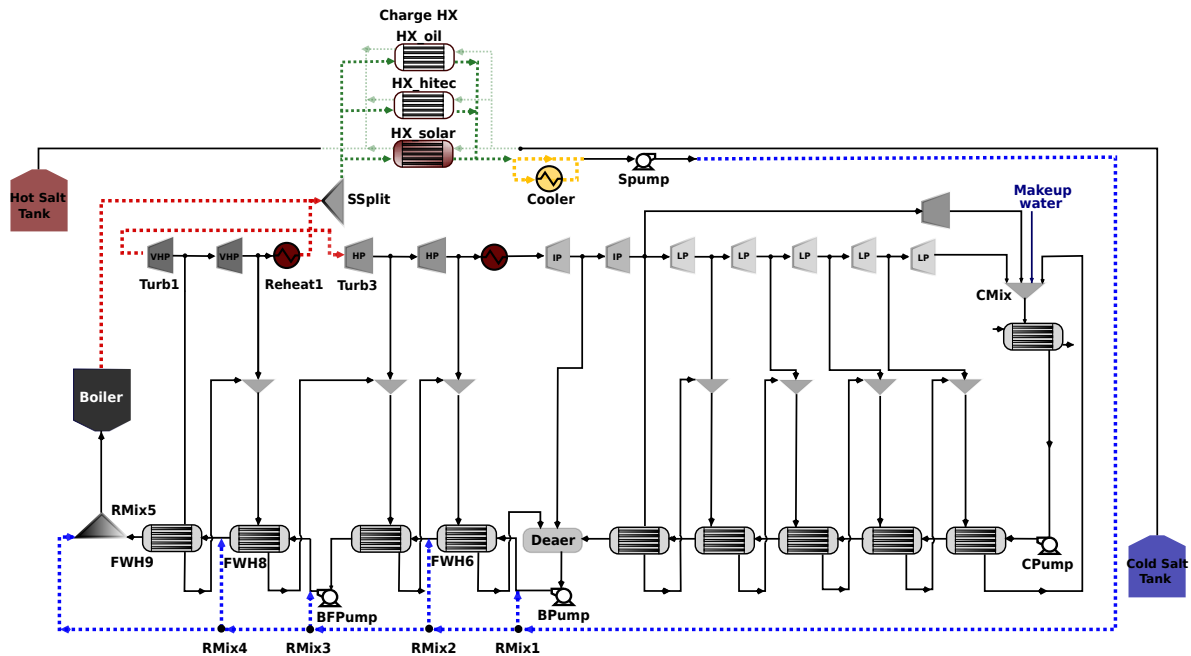
Table 3 summarizes how the charge design decisions (Table 2) are modeled using the equations in Disjunctions 1a to 1d. Each disjunction considers multiple alternatives, resulting in the exploration of 60 different configurations for the proposed charge GDP superstructure. The notation in the Disjunctions 1a to 1d is: $h(x, d)$ represents all equality constraints (mass and energy balances and performance equations) for the unit equipment given in the superscript, Y represents the state

variables (flow, pressure, and enthalpy) of the unit equipment in the superscript, in and out are the inlet and outlet streams of the unit equipment given in the superscript, p is the pressure of the stream and unit equipment in the subscript and superscript, respectively, and Solar, Hitec, and oil are the storage material alternatives for the storage heat exchangers.

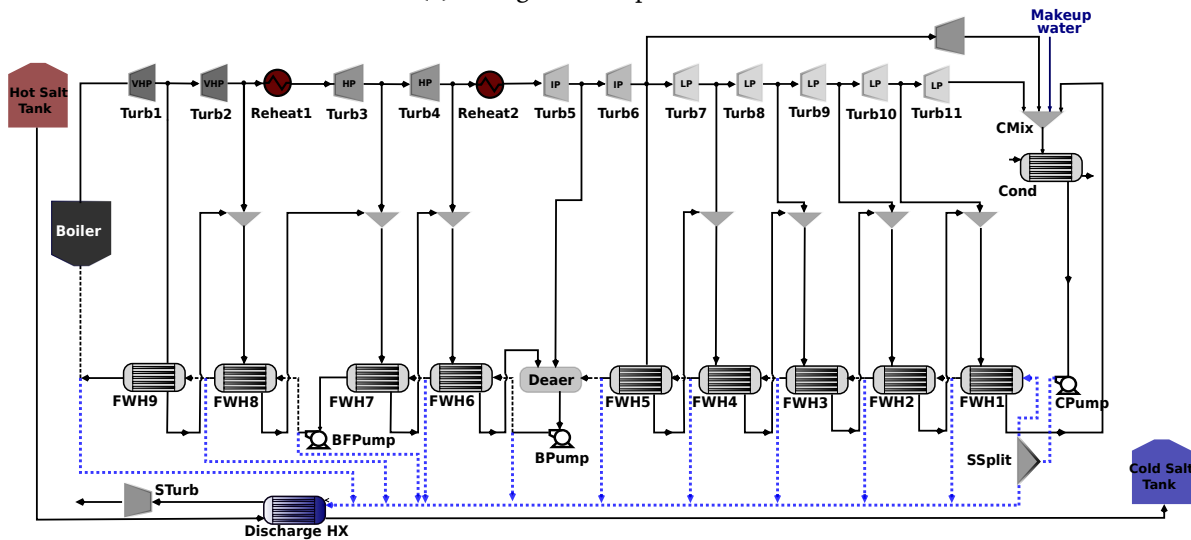
Table 2: Discrete design decisions in charge and discharge GDP superstructures.

Number	Charge Discrete Design Decision
1	Storage material in the heat exchanger
2	Steam source within the power plant
3	Point for the return of the condensed steam to the power plant cycle
4	Addition of a cooler after the charge cycle

Number	Discharge Discrete Design Decision
1	Extraction point of condensed steam



(a) Charge GDP superstructure.



(b) Discharge GDP superstructure.

Figure 4: Process flowsheet for the (a) charge and (b) discharge GDP superstructures of the ultra-supercritical plant. The flowsheets include colored dashed lines that represent the design alternatives for each design decision or disjunction. In (a) or charge superstructure, the disjunction 1 and its alternatives are shown as green dashed lines, disjunction 2 as red dashed lines, disjunction 3 as blue dashed lines, and disjunction 4 as yellow dashed lines. In (b) or discharge superstructure, the disjunction 1 and its eleven alternatives are shown as the blue dashed lines.

For the discharge GDP superstructure in Figure 4b, where the energy stored during the charge process is used to reheat condensed steam extracted from the plant to produce power, we consider one

disjunction for the selection of an extraction point of condensed steam from the plant. Figure 4b shows this as blue dashed lines. Table 4 summarizes how the discharge design decision (Table 2) is modeled using Disjunction 1g, which considers 11 alternatives for the extraction of condensate from the plant. Disjunction 1g follows the same notation described in the charge superstructure. Considering the discharge process and its auxiliary units in Figure 3b, in the discharge GDP superstructure we connect a storage turbine to the outlet of the discharge heat exchanger to produce extra power. Note that the condensate at the outlet of this storage turbine is not explicitly recycled back to the plant, but it is assumed to be added as make-up water in the condenser mixer (CMix) of the power plant. Therefore, there is no need to recycle steam condensate to the power plant. Additionally, since we assume both charge and discharge heat exchangers use the same storage material and this is already a discrete decision in the charge GDP superstructure, we do not include this as a discrete design decision in the discharge design superstructure.

Table 3: Description of design decisions as disjunctions in charge GDP superstructure.

Disjunction		Design Decisions	Alternatives (Disjuncts)	Boolean Variable	Representation in Figure 4a
Number	Equation				
1	1a	Storage Material	Solar salt HX Hitec salt HX Thermal oil HX	$z_{1,1}^{\text{charge}}$ $z_{1,2}^{\text{charge}}$ $z_{1,3}^{\text{charge}}$	Green dashed lines
2	1b	Steam source	Boiler outlet (VHP source) Reheat ₁ outlet (HP source)	$z_{2,1}^{\text{charge}}$ $z_{2,1}^{\text{charge}}$ $z_{2,2}^{\text{charge}}$	Red dashed lines
3	1c	Return of condensed steam	FWH ₆ inlet 1 FWH ₇ inlet 1 FWH ₈ inlet 1 FWH ₉ inlet 1 Boiler inlet	$z_{3,1}^{\text{charge}}$ $z_{3,2}^{\text{charge}}$ $z_{3,3}^{\text{charge}}$ $z_{3,4}^{\text{charge}}$ $z_{3,5}^{\text{charge}}$	Blue dashed lines
4	1d	Cooler after storage	Add cooler No cooler	$z_{4,1}^{\text{charge}}$ $z_{4,2}^{\text{charge}}$	Yellow dashed lines

Table 4: Description of design decisions as disjunctions in discharge GDP superstructure.

Disjunction		Design Decision	Alternatives (Disjuncts)	Boolean Variable	Representation in Figure 4b
Number	Equation				
1	1g	Condensed Steam Source	CPump outlet FWH ₁ outlet 1 FWH ₂ outlet 1 FWH ₃ outlet 1 FWH ₄ outlet 1 FWH ₅ outlet 1 BPumpoutlet FWH ₆ outlet 1 BFPump outlet FWH ₈ outlet 1 FWH ₉ outlet	$z_1^{\text{discharge}}$ $z_2^{\text{discharge}}$ $z_3^{\text{discharge}}$ $z_4^{\text{discharge}}$ $z_5^{\text{discharge}}$ $z_6^{\text{discharge}}$ $z_7^{\text{discharge}}$ $z_8^{\text{discharge}}$ $z_9^{\text{discharge}}$ $z_{10}^{\text{discharge}}$ $z_{11}^{\text{discharge}}$	Blue dashed lines

$$\left[\begin{array}{c} \text{charge} \\ z_{1,1} \\ h(x^{\text{HXSolar}}, d^{\text{HXSolar}}) = 0 \\ Y_{\text{in}}^{\text{SPump}} = Y_{\text{out}}^{\text{HXSolar}} \end{array} \right] \vee \left[\begin{array}{c} \text{charge} \\ z_{1,2} \\ h(x^{\text{HXHitec}}, d^{\text{HXHitec}}) = 0 \\ Y_{\text{in}}^{\text{SPump}} = Y_{\text{out}}^{\text{HXHitec}} \end{array} \right] \vee \left[\begin{array}{c} \text{charge} \\ z_{1,3} \\ h(x^{\text{HXoil}}, d^{\text{HXoil}}) = 0 \\ Y_{\text{in}}^{\text{SPump}} = Y_{\text{out}}^{\text{HXoil}} \end{array} \right] \quad (1a)$$

$$\left[\begin{array}{c} \text{charge} \\ z_{2,1} \\ h(x^{\text{SSP}}, d^{\text{SSP}}) = 0 \\ Y_{\text{in}}^{\text{SSP}} = Y_{\text{out}}^{\text{Boiler}} \\ Y_{\text{in}}^{\text{HX}_i} = Y_{\text{out}_1}^{\text{SSP}} \\ Y_{\text{in}}^{\text{Turb}_1} = Y_{\text{out}_2}^{\text{SSP}} \end{array} \right] \vee \left[\begin{array}{c} \text{charge} \\ z_{2,2} \\ h(x^{\text{SSP}}, d^{\text{SSP}}) = 0 \\ Y_{\text{in}}^{\text{SSP}} = Y_{\text{out}}^{\text{Reheat}_1} \\ Y_{\text{in}}^{\text{HX}_i} = Y_{\text{out}_1}^{\text{SSP}}, \forall i \in \mathcal{S} \\ Y_{\text{in}}^{\text{Turb}_3} = Y_{\text{out}_2}^{\text{SSP}} \end{array} \right] \quad (1b)$$

$$\left[\begin{array}{c} \text{charge} \\ z_{3,1} \\ h(x^{\text{RMix}_1}, d^{\text{RMix}_1}) = 0 \\ Y_{\text{in}_1}^{\text{RMix}_1} = Y_{\text{out}}^{\text{SPump}} \\ Y_{\text{in}_2}^{\text{RMix}_1} = Y_{\text{out}}^{\text{BPump}} \\ Y_{\text{in}_1}^{\text{FWH}_6} = Y_{\text{out}}^{\text{RMix}_1} \\ p_{\text{out}}^{\text{RMix}_1} = f(p) \end{array} \right] \vee \left[\begin{array}{c} \text{charge} \\ z_{3,2} \\ h(x^{\text{RMix}_2}, d^{\text{RMix}_2}) = 0 \\ Y_{\text{in}_1}^{\text{RMix}_2} = Y_{\text{out}}^{\text{SPump}} \\ Y_{\text{in}_2}^{\text{RMix}_2} = Y_{\text{out}_1}^{\text{FWH}_6} \\ Y_{\text{in}_1}^{\text{FWH}_7} = Y_{\text{out}}^{\text{RMix}_2} \\ p_{\text{out}}^{\text{RMix}_2} = f(p) \end{array} \right] \vee \left[\begin{array}{c} \text{charge} \\ z_{3,3} \\ h(x^{\text{RMix}_3}, d^{\text{RMix}_3}) = 0 \\ Y_{\text{in}_1}^{\text{RMix}_3} = Y_{\text{out}}^{\text{SPump}} \\ Y_{\text{in}_2}^{\text{RMix}_3} = Y_{\text{out}}^{\text{BFPump}} \\ Y_{\text{in}_1}^{\text{FWH}_8} = Y_{\text{out}}^{\text{RMix}_3} \\ p_{\text{out}}^{\text{RMix}_3} = f(p) \end{array} \right] \vee$$

$$\left[\begin{array}{c} \text{charge} \\ z_{3,4} \\ h(x^{\text{RMix}_4}, d^{\text{RMix}_4}) = 0 \\ Y_{\text{in}_1}^{\text{RMix}_4} = Y_{\text{out}}^{\text{SPump}} \\ Y_{\text{in}_2}^{\text{RMix}_4} = Y_{\text{out}_1}^{\text{FWH}_8} \\ Y_{\text{in}_1}^{\text{FWH}_9} = Y_{\text{out}}^{\text{RMix}_4} \\ p_{\text{out}}^{\text{RMix}_4} = f(p) \end{array} \right] \vee \left[\begin{array}{c} \text{charge} \\ z_{3,5} \\ h(x^{\text{RMix}_5}, d^{\text{RMix}_5}) = 0 \\ Y_{\text{in}_1}^{\text{RMix}_5} = Y_{\text{out}}^{\text{SPump}} \\ Y_{\text{in}_2}^{\text{RMix}_5} = Y_{\text{out}_1}^{\text{FWH}_9} \\ Y_{\text{in}}^{\text{Boiler}} = Y_{\text{out}}^{\text{RMix}_5} \\ p_{\text{out}}^{\text{RMix}_5} = f(p) \end{array} \right] \quad (1c)$$

$$\left[\begin{array}{c} \text{charge} \\ z_{4,1} \\ h(x^{\text{Cooler}}, d^{\text{Cooler}}) = 0 \\ Y_{\text{in}}^{\text{Cooler}} = Y_{\text{out}}^{\text{HX}_s}, \forall s \in \mathcal{S} \\ Y_{\text{in}}^{\text{SPump}} = Y_{\text{out}}^{\text{Cooler}} \end{array} \right] \vee \left[\begin{array}{c} \text{charge} \\ z_{4,2} \\ Y_{\text{in}}^{\text{SPump}} = Y_{\text{out}}^{\text{HX}_s}, \forall s \in \mathcal{S} \end{array} \right] \quad (1d)$$

$$\mathcal{S} = [\text{Solar}, \text{Hitec}, \text{oil}] \quad (1e)$$

$$p(x) = \min(p_{\text{in}_1}^{\text{RMix}}, p_{\text{in}_2}^{\text{RMix}}) \quad (1f)$$

$$\left[\begin{array}{c} \text{discharge} \\ z_1 \\ Y_{\text{out}}^{\text{SSP}} = Y_{\text{out}}^{\text{CPump}} \\ Y_{\text{in}_1}^{\text{FWH}_1} = Y_{\text{out}_2}^{\text{SSP}} \\ Y_{\text{in}}^{\text{HX}^*} = Y_{\text{out}_1}^{\text{SSP}} \\ Y_{\text{in}}^{\text{STurb}} = Y_{\text{out}}^{\text{HX}^*} \end{array} \right] \vee \left[\begin{array}{c} \text{discharge} \\ z_2 \\ Y_{\text{out}_1}^{\text{SSP}} = Y_{\text{out}_1}^{\text{FWH}_1} \\ Y_{\text{in}_1}^{\text{FWH}_2} = Y_{\text{out}_2}^{\text{SSP}} \\ Y_{\text{in}}^{\text{HX}^*} = Y_{\text{out}_1}^{\text{SSP}} \\ Y_{\text{in}}^{\text{STurb}} = Y_{\text{out}}^{\text{HX}^*} \end{array} \right] \vee \left[\begin{array}{c} \text{discharge} \\ z_3 \\ Y_{\text{out}_1}^{\text{SSP}} = Y_{\text{out}_1}^{\text{FWH}_2} \\ Y_{\text{in}_1}^{\text{FWH}_3} = Y_{\text{out}_2}^{\text{SSP}} \\ Y_{\text{in}}^{\text{HX}^*} = Y_{\text{out}_1}^{\text{SSP}} \\ Y_{\text{in}}^{\text{STurb}} = Y_{\text{out}}^{\text{HX}^*} \end{array} \right] \vee \left[\begin{array}{c} \text{discharge} \\ z_4 \\ Y_{\text{out}_1}^{\text{SSP}} = Y_{\text{out}_1}^{\text{FWH}_3} \\ Y_{\text{in}_1}^{\text{FWH}_4} = Y_{\text{out}_2}^{\text{SSP}} \\ Y_{\text{in}}^{\text{HX}^*} = Y_{\text{out}_1}^{\text{SSP}} \\ Y_{\text{in}}^{\text{STurb}} = Y_{\text{out}}^{\text{HX}^*} \end{array} \right] \vee$$

$$\begin{aligned}
& \left[\begin{array}{c} \text{discharge} \\ z_5 \\ Y_{\text{SSP}}^{\text{out}_1} = Y_{\text{FWH}_4}^{\text{out}_1} \\ Y_{\text{in}_1}^{\text{FWH}_5} = Y_{\text{out}_2}^{\text{SSP}} \\ Y_{\text{in}}^{\text{HX}^*} = Y_{\text{out}_1}^{\text{SSP}} \\ Y_{\text{in}}^{\text{STurb}} = Y_{\text{out}}^{\text{HX}^*} \end{array} \right] \vee \left[\begin{array}{c} \text{discharge} \\ z_6 \\ Y_{\text{SSP}}^{\text{out}} = Y_{\text{FWH}_5}^{\text{out}} \\ Y_{\text{in}_1}^{\text{Deaer}} = Y_{\text{out}_2}^{\text{SSP}} \\ Y_{\text{in}}^{\text{HX}^*} = Y_{\text{out}_1}^{\text{SSP}} \\ Y_{\text{in}}^{\text{STurb}} = Y_{\text{out}}^{\text{HX}^*} \end{array} \right] \vee \left[\begin{array}{c} \text{discharge} \\ z_7 \\ Y_{\text{SSP}}^{\text{out}} = Y_{\text{BPump}}^{\text{out}} \\ Y_{\text{in}_1}^{\text{FWH}_6} = Y_{\text{out}_2}^{\text{SSP}} \\ Y_{\text{in}}^{\text{HX}^*} = Y_{\text{out}_1}^{\text{SSP}} \\ Y_{\text{in}}^{\text{STurb}} = Y_{\text{out}}^{\text{HX}^*} \end{array} \right] \vee \left[\begin{array}{c} \text{discharge} \\ z_8 \\ Y_{\text{SSP}}^{\text{out}_1} = Y_{\text{FWH}_6}^{\text{out}_1} \\ Y_{\text{in}_1}^{\text{FWH}_7} = Y_{\text{out}_2}^{\text{SSP}} \\ Y_{\text{in}}^{\text{HX}^*} = Y_{\text{out}_1}^{\text{SSP}} \\ Y_{\text{in}}^{\text{STurb}} = Y_{\text{out}}^{\text{HX}^*} \end{array} \right] \\
& \left[\begin{array}{c} \text{discharge} \\ z_9 \\ Y_{\text{SSP}}^{\text{out}} = Y_{\text{BFPump}}^{\text{out}} \\ Y_{\text{in}_1}^{\text{FWH}_8} = Y_{\text{out}_2}^{\text{SSP}} \\ Y_{\text{in}}^{\text{HX}^*} = Y_{\text{out}_1}^{\text{SSP}} \\ Y_{\text{in}}^{\text{STurb}} = Y_{\text{out}}^{\text{HX}^*} \end{array} \right] \vee \left[\begin{array}{c} \text{discharge} \\ z_{10} \\ Y_{\text{SSP}}^{\text{out}_1} = Y_{\text{FWH}_8}^{\text{out}_1} \\ Y_{\text{in}_1}^{\text{FWH}_9} = Y_{\text{out}_2}^{\text{SSP}} \\ Y_{\text{in}}^{\text{HX}^*} = Y_{\text{out}_1}^{\text{SSP}} \\ Y_{\text{in}}^{\text{STurb}} = Y_{\text{out}}^{\text{HX}^*} \end{array} \right] \vee \left[\begin{array}{c} \text{discharge} \\ z_{11} \\ Y_{\text{SSP}}^{\text{out}_1} = Y_{\text{FWH}_9}^{\text{out}_1} \\ Y_{\text{Boiler}}^{\text{in}} = Y_{\text{out}_2}^{\text{SSP}} \\ Y_{\text{in}}^{\text{HX}^*} = Y_{\text{out}_1}^{\text{SSP}} \\ Y_{\text{in}}^{\text{STurb}} = Y_{\text{out}}^{\text{HX}^*} \end{array} \right] \quad (1g)
\end{aligned}$$

To determine the optimal point to integrate the charge heat exchanger with the USCPP while considering multiple viable process streams using disjunctions as the discrete design decisions, we propose the GDP optimization problem in Equations 2a to 2f to show how, with the use of optimization-based design techniques, we can integrate TES with fossil-fueled generators while increasing their economic benefits and performance.

$$\min \quad REV(\pi^{\text{charge}}) - OPEX - CAPEX^{\text{charge}} \quad (2a)$$

$$\text{s.t.} \quad h(x^{\text{charge}}, d^{\text{charge}}) = 0 \quad (2b)$$

$$g(x^{\text{charge}}, d^{\text{charge}}) \leq 0 \quad (2c)$$

$$\text{Disjunctions 1a to 1d} \quad (2d)$$

$$z_{i,k}^{\text{charge}} \in \{\text{True}, \text{False}\}, \forall i \in \mathcal{Z}, \forall k \in \mathcal{K} \quad (2e)$$

$$x^{\text{charge,lb}} \leq x^{\text{charge}} \leq x^{\text{charge,ub}}, \forall x \in \mathcal{X} \subseteq \mathbb{R}^n \quad (2f)$$

In this charge GDP design problem, we maximize a net profit function calculated considering the revenue function (REV), operating costs ($OPEX$), and capital costs ($CAPEX$) of the USCPP and storage system, as shown in Equation 2a. The revenue is calculated assuming a fixed value for the electricity price of $\pi^{\text{charge}} = \$22$ per MWh, which is similar to the average π value for the time horizons used in this study. The $OPEX$ includes the fixed and variable costs for the power plant and fuel consumption. The $CAPEX^{\text{charge}}$ considers annualized costs for the plant and charge storage system, including the cost of the charge heat exchangers, storage material pumps, and the insulated tank needed to store the storage material. We use the IDAES[®] costing framework to calculate capital costs, which considers assumptions given in [32]. Equations 2b and 2c represent the model and performance equations of the USCPP and charge storage process, including mass and energy balances and process specification equations that depend on the set of continuous variables x^{charge} in the charge process, given design parameters d^{charge} , and all unit models used to construct the USCPP and the charge process (see Section 2.3). Since each point for the connection of the charge storage heat exchanger and its auxiliary units with the USCPP is considered a design decision and added to the model as a disjunction, we include Equation 2d to the optimization problem that comprises the four design decisions for the charge process given in Equations 1a to 1d. The decision of the selection of an alternative in each disjunction is represented with the Boolean variable z that can take the value of *True* or *False* in the disjunction equations as given in

Equation 2e. Since each disjunction contains multiple alternatives (or disjuncts k), we enforce that one and only one of the alternatives is *True*, which implies that when one alternative is selected, the other alternatives must be *False*. For example, if the Boolean variable $z_{1,1}^{\text{charge}}$ in Equation 1a is *True*, the equations and constraints for this alternative are included in the global model equations. The other alternatives, $z_{1,2}^{\text{charge}}$ and $z_{1,3}^{\text{charge}}$, must then take the value of *False* and are not included in the superstructure model. This is enforced with the logical exclusive OR relationship " \vee " in the disjunctions equations. \mathcal{Z} in Equation 2e represents the set of disjunctions z , while \mathcal{K} represents the set of disjuncts k for each disjunction z . Finally, Equation 2f specifies the lower and upper bounds ($x^{\text{charge,lb}}$ and $x^{\text{charge,ub}}$, respectively) for all the continuous variables x in the set of variables \mathcal{X} in the model. Once defined, this mathematical formulation is used for the solution of the charge GDP superstructure.

For the discharge GDP design problem, we formulate an optimization problem analogous to the charge GDP problem (Equations 2a to 2f). Equations 3a to 3f show the discharge GDP model formulation proposed to determine the optimal points of integration of the discharge heat exchanger and its auxiliary units within the USCPP.

$$\min \quad REV(\pi^{\text{discharge}}) - OPEX - CAPEX^{\text{discharge}} \quad (3a)$$

$$\text{s.t.} \quad h(x^{\text{discharge}}, d^{c,\text{charge}}, d^{\text{charge}}) = 0 \quad (3b)$$

$$g(x^{\text{discharge}}, d^{c,\text{charge}}) \leq 0 \quad (3c)$$

$$\text{Disjunction 1g} \quad (3d)$$

$$z_k^{\text{discharge}} \in \{\text{True}, \text{False}\}, \forall k \in \mathcal{K} \quad (3e)$$

$$x^{\text{discharge,lb}} \leq x^{\text{discharge}} \leq x^{\text{discharge,ub}}, \forall x \in \mathcal{X} \subseteq \mathbb{R}^n \quad (3f)$$

In this formulation, we also maximize a profit function, but this differs from the charge formulation in the electricity price used in Equation 3a for the calculation of revenue, which has a value of $\pi^{\text{discharge}} = \40 per MWh for the discharge problem, and is similar to the highest π observed in the longest time horizon of 168 hours used in this study, and considers the power produced by both the power plant and storage turbine, $CAPEX^{\text{discharge}}$ that considers annualized costs for the plant and discharge storage system, Equations 3b and 3c that include the model and performance equations of the USCPP and discharge process, and the discrete design decision as a disjunction in Equation 3d that specifies the connection to the power plant for the extraction of condensed steam. Since we use the same storage material used in the charge GDP superstructure, the discharge model Equations 3b and 3c require data from the storage material selected during the solution of the charge GDP superstructure. To obtain this data, the charge and discharge GDP superstructures are solved sequentially, starting with the charge GDP superstructure to determine the storage material (type and amount) and its operating temperature. These values are saved and used for the solution of the discharge superstructure.

The model for the charge superstructure has 795 constraints and 729 variables of which 12 are binary. The discharge superstructure has 664 constraints and 566 variables of which 6 are binary. Since we want to explore the entire set of configurations for each superstructure, we use GDPopt [9] with RIC (or reduced integer cuts) as the algorithm strategy. The flowsheets are initialized using the IDAES[®] initialization procedure that propagates state variables through connected units.

Step 2: Optimization Formulation of Multi-period under Price-taker Assumption

Once the GDP superstructures in Step 1 are solved, we obtain the optimal discrete design decisions d^d and use them to construct the model of an integrated USCPP. This integrated plant includes the storage charge and discharge processes within the same USCPP to offer the flexibility of storing and using energy when one or the other operation is desired. Since both storage processes are included in the same USCPP model, we include a minimum work constraint for each heat exchanger to avoid zero flows in the TES system. To achieve this, we add a lower bound for the heat duty of each storage heat exchanger to be greater than a small non-zero value (i.e., 10 MWth). This simplification allows the heat exchangers to be in a warm start state and enables a better convergence of the mathematical models.

A multi-period simultaneous design and operation problem is formulated using the integrated USCPP model for an objective of maximizing profit considering the time-varying electricity prices under a price-taker assumption as shown in Equations 4a to 4l.

$$\min \sum_{t=1}^{\mathcal{T}} (REV_t - OPEX_t) - CAPEX \quad (4a)$$

$$\text{s.t. } REV_t = P_t^{\text{total}} \pi_t, \forall t \in \mathcal{T} \quad (4b)$$

$$OPEX_t = F_t^{\text{coal}} C_t^{\text{coal}}, \forall t \in \mathcal{T} \quad (4c)$$

$$CAPEX_t = f(d, F_t^{\text{water}}, F_t^{\text{smaterial}}), \forall t \in \mathcal{T} \quad (4d)$$

$$h(x_t, d) = 0, \forall t \in \mathcal{T} \quad (4e)$$

$$P_{t-1}^{\text{total}} - \rho \leq P_t^{\text{total}}, \forall t \in \mathcal{T} \quad (4f)$$

$$P_{t-1}^{\text{total}} + \rho \geq P_t^{\text{total}}, \forall t \in \mathcal{T} \quad (4g)$$

$$I_t^{\text{hot}} = I_{t-1}^{\text{hot}} + 3600 (F_t^{\text{smaterial,charge}} - F_t^{\text{smaterial,discharge}}), \forall t \in \mathcal{T} \quad (4h)$$

$$I^{\text{total}} = I_t^{\text{hot}} + I_t^{\text{cold}}, \forall t \in \mathcal{T} \quad (4i)$$

$$N_{t+1}^d = N_t^d, \forall t \in \{1, \dots, n-1\} \quad (4j)$$

$$I_n^{\text{hot}} = I_1^{\text{hot}} \quad (4k)$$

$$x^{\text{lb}} \leq x \leq x^{\text{ub}}, \forall x \in \mathcal{X} \subseteq \mathbb{R}^n \quad (4l)$$

In the multi-period optimization model, we maximize a net profit function in Equation 4a, which calculates the total profit of the energy system considering the revenue and costs over one-hour time steps t in the set of time periods \mathcal{T} . We consider a rigorous model of an integrated USCPP for each time period, which involves 607 variables, 601 equations, and 12 constraints that include multiple nonlinear expressions that describe the mass, energy, and thermal properties of the system. We calculate the revenue using Equation 4b, where we consider average electricity prices π_t^{average} and the total power produced by the integrated power plant or P_t^{total} at each time step $t \in \mathcal{T}$. The costs include $OPEX$ and $CAPEX$ expenses associated with the power plant and TES system. We calculate the capital costs based on given design parameters for the unit operations (i.e., heat exchangers, pumps, storage tanks, material inventory, etc.) using the IDAES[®] Unit Costing library, and we annualize these over a 30-year power plant lifetime. In Equation 4e we include first-principle and nonlinear equations that describe the integrated USCPP model and are time-indexed to enforce mass and energy balances and performance equations of the unit equipment models

over the time steps. Refer to Section 2.3 for more details about the USCPP and TES system models. We include ramping constraints in Equations 4f and 4g, assuming a ramping rate ρ of 1 MW/min and two mass balance equations in Equations 4h and 4i to calculate the amount of available hot and cold storage material (I) at the end of each time period considering the flow (F) of storage material that enters and leaves each storage tank. In this optimization problem, the simultaneous design and operation of the integrated USCPP is possible due to the addition of the nonanticipativity constraints in Equation 4j, which ensure that the calculated continuous design decisions d^c (area of storage heat exchangers and temperature of storage material), have the same value at all time periods. We include a periodicity constraint in Equation 4k to ensure that the initial and final (end of horizon n) states of the hot storage tank are the same. Finally, we include bounds for the variables x as shown in Equation 4l. This formulation does not consider the dispatch load from the market. Instead, it considers the economic signal from the market, so the integrated energy system can only tell the grid when it can operate and how much energy it can provide, if needed.

With the use of the Multiperiod model in IDAES[®], we are able to generate a global model that contains a series of steady-state models of the integrated USCPP that are connected to each other using coupling variables and nonanticipativity constraints. Figure 5 shows a graphical representation of this multi-period step approach. Considering the multi-period model, we create an instance for each integrated USCPP, one for each time period, to construct a global model that contains multiple steady-state models of the integrated USCPP. Each instance of the integrated USCPP model is initialized using an identical steady-state solution with the same heat duties for charge and discharge heat exchangers of TES. As the steady solution also offers a feasible solution to the linking constraints and periodic conditions, this method of initialization offers an initial feasible solution for the multi-period model. When considering the integration of TES and the effect of the electricity market in this multi-period model, we aim to enable the power plant to shift its power generation from a charge, discharge, or no storage process. This way, the integrated power plant can avoid generating energy at periods of low energy prices and increase energy generation during the highest value hours to maximize profit. For a 24-hour period instance of the multi-period model, the simultaneous design model has 14,679 variables and 14,892 constraints, including 312 inequality constraints.

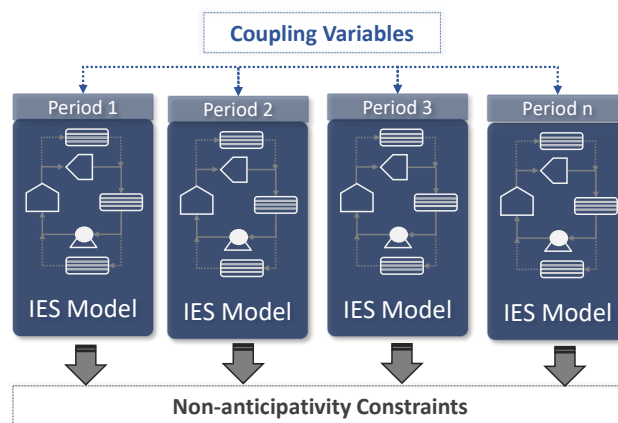


Figure 5: Step 2 or multi-period step approach for the simultaneous design and operation of the integrated ultra-supercritical power plant.

3. Results

In this section, we demonstrate the two-step approach by retrofitting an USCPP with TES.

3.1 Step 1: Generalized Disjunctive Programming Design

Charge Superstructure Results

Table 5 shows the results for the top seven feasible designs (rank 1 to 7) and the last feasible design (rank 55) for the charge superstructure. In Table 5, the profit (as the objective function) has a negative value, which means that the electricity price during charge ($\pi^{\text{charge}} = \$22$ per MWh) is low compared to the operating and capital costs of the plant. This is an incentive to use the charge process in the integrated USCPP since it is more efficient for producing additional electricity and storing it as compared to turning down the plant, causing the plant to operate far from the base load.

Table 5: Results for the discrete and continuous design decisions for the top seven feasible designs and the last feasible design for the charge GDP superstructure of the ultra-supercritical power plant.

Rank	Discrete Decisions				Area HX (m ²)	Hot Salt Temp. (K)	Profit (\$/hour)
	Storage Material	Steam Source	Condensate Return	Cooling			
1	Solar	Reheat ₁	Boiler	No	1,890.12	826.56	-1,584.57
2	Solar	Reheat ₁	Boiler	Yes	1,890.12	826.56	-1,584.68
3	Solar	Reheat ₁	FWH ₉	No	1,890.12	826.56	-1,584.87
4	Solar	Reheat ₁	FWH ₉	Yes	1,890.12	826.56	-1,584.98
5	Solar	Reheat ₁	FWH ₈	No	1,890.12	826.56	-1,587.77
6	Solar	Reheat ₁	FWH ₈	Yes	1,890.12	826.56	-1,587.88
7	Solar	Reheat ₁	FWH ₇	No	2,004.89	822.07	-1,598.19
55 ^a	Thermal oil	Boiler	FWH ₇	Yes	2,218.66	616.00	-1,775.71

^a 55 out of the 60 explored configurations are feasible

For the top seven feasible designs in Table 5, we observe differences of less than 1% in terms of profit since they all select the Solar salt as the storage material and the HP steam source. In these feasible designs, the selected Solar salt is heated using an HP steam source withdrawn from the Reheat₁ at a pressure of approximately 8 MPa and temperature of 866.15 K. For the top six feasible designs, the Solar salt is heated in a heat exchanger with the same area of 1,890.12 m² at a rate

of 150 MW. Since the charge heat exchanger uses the HP steam source, the Solar salt increases its temperature in the charge heat exchanger from an initial temperature of 513.15 K to 826.56 K using a steam flow from the Reheat₁ of about 3,570 mol/s and a total amount of purchased salt of about 6,840 metric tonnes. For the rank 1 feasible design, we find that once the steam is exhausted, it is mixed with the flow from the FWH₉ outlet and sent back to the boiler inlet without the need for a cooler after the charge heat exchanger.

The small differences observed in the profit values of the top seven designs in Table 5 derive from the selection of different points in the feed water train for the return of the condensed steam while interchangeably selecting the use of a cooler. We compared these feasible designs to further understand these differences and to define the effects that the different discrete design decisions have on the profit. The main observations drawn from this analysis are given below:

Condensed steam return and cooler selection: The profit is maximized when the condensed steam is returned to the high-pressure feed water train, with the flexibility of selecting multiple points for the condensed steam return without drastic differences in the profit. In addition, the use of a cooler and the effect it has on the profit directly relates to its energy duty and capital cost. This is observed when comparing the rank 2 feasible design with rank 1, where we see that rank 2 has the same configuration as rank 1, with the exception of the addition of a cooler after the charge storage process. Since this added cooler has a negligible heat duty and a relatively small capital cost, the rank 2 solution has a profit similar to that of rank 1 (small capital cost).

Storage material: The selection of storage material has the most impact on the profit value since the price of storage material directly affects the capital cost. The difference is relevant because each storage material has a different price (i.e., \$0.49 per kg for Solar salt, \$0.93 per kg for Hitec salt, and \$6.72 per kg for thermal oil) with a varying range of operating temperatures. Comparing all the feasible designs, we found that the least profitable configurations resulted in charge heat exchangers that used thermal oil as the storage material. This is observed when comparing rank 1 with the last rank 55 solution in Table 5, where we have a maximum difference of about 10% in terms of profit. In fact, a comparison of all feasible designs in Figure 10a in Appendix D sheds light on the relative impact that the storage material has on the profit.

Steam source: The steam source has a significant impact on the profit since it affects the heat exchanger area and thus the capital cost. This is related to the value of the specific enthalpy of steam and is explained when studying the Mollier diagram for supercritical steam. This diagram shows that the VHP steam (i.e., inlet to Turb₁) has a lower specific enthalpy of 61.5 kJ/mol when compared to the HP steam (i.e., inlet to Turb₃) that has a value of 65.2 kJ/mol. Thus, the Solar salt, when heated using an HP steam source from the boiler outlet at a higher specific enthalpy, is more efficient and profitable than the VHP steam source. Figure 10b in Appendix D shows the effect of the steam source in the areas of the charge heat exchanger for all feasible designs, where we observe that for the Solar salt and thermal oil the areas of the heat exchangers are smaller when the HP steam source is selected, while for the Hitec salt the area values vary slightly between steam sources. Note that there is no clear trend for the area between the storage materials since the size of the heat exchanger depends on other continuous design variables such as temperature bounds for the storage material, steam flow, salt flow, and amount of available salt for each storage material.

Finally, considering only the rank 1 design, we built an USCPP integrated with the charge process. Figure 6a shows this optimal charge configuration.

Discharge Superstructure Results

Table 6 shows the results for the discharge GDP superstructure for the top seven feasible designs (rank 1 to 7) and the last feasible design (rank 11). In the discharge superstructure, we use Solar salt as the storage material at the same hot temperature of 826.56 K found during the solution of the charge superstructure

Table 6: Results for the discrete and continuous design decisions for the top seven and last feasible designs for the discharge GDP superstructure for the ultra-supercritical power plant. The variables marked with an * are variables that have a fixed value during the optimization.

Rank	Discrete Decision	Area HX (m ²)	Hot Salt Temp. (K)	Profit (\$/hour)
	Condensed Steam From Outlet			
1	CPump	436.44	826.56*	11,670.79
2	FWH ₁	535.24	826.56*	11,669.17
3	FWH ₂	751.84	826.56*	11,664.12
4	FWH ₃	921.22	826.56*	11,658.44
5	FWH ₄	1,154.35	826.56*	11,648.12
6	FWH ₅	1,678.90	826.56*	11,617.34
7	BPump	2,079.26	826.56*	11,596.50
11	FWH ₉	5,000.00	826.56*	11,301.60

The most profitable designs in Table 6 involve the extraction of condensed steam coming from the low-pressure feed water train. In the rank 1 feasible design, the discharge heat exchanger uses the Solar salt to reheat a fraction of the condensed steam from the CPump outlet using a flow of about 2,918 mol/s of condensed steam in a discharge heat exchanger with an area of 436.44 m² at a heat duty of 148.50 MW. The condensed steam is heated from 312 K to 562 K. The reheated steam, now at a higher temperature and pressure of 2 MPa, is fed to the storage turbine to produce additional power of about 40 MW. As a fraction of the steam from the thermal cycle is taken out of the CPump, the same amount of water is added as makeup water in the condenser mixer CMix to maintain the steam flow rates. When comparing the charge and discharge heat exchanger areas, we observe that the discharge heat exchanger is smaller than the charge heat exchanger (436.44 m² vs. 1,890.12 m², respectively). This difference is due to the smaller feed water flow that goes through the discharge heat exchanger when compared to the flow in the charge heat exchanger.

While exploring the different feasible configurations in Table 6, we observe the effect that the extraction point for the condensed steam has on the profit. The main observations are given below:

Condensed steam source. The profit increases when using condensed steam from the low-pressure feed water train since this affects the size of the discharge heat exchanger and thus the capital cost. Figure 11a in Appendix D shows a comparison of the profit for all the feasible designs. For example, a comparison between the rank 1 and rank 2 feasible designs shows a difference in terms of profit of less than 0.1%. This difference is due to an increment in the area of the heat exchangers (rank 2 design uses a bigger discharge heat exchanger of 535.24 m²). The highest difference in profit is about 3%, which is observed when comparing the rank 1 to the rank 11 feasible design (also included in Table 6), and it is also due to the increment in the area of the discharge heat exchanger. When comparing Figures 11a and 11b in Appendix D, we observe a correlation between profit and the area of the heat exchangers, where we observe that the profit increments when the area of the discharge heat exchanger decreases.

Finally, considering the rank 1 feasible design, we built the optimal discharge USCPP superstructure in Figure 6b.

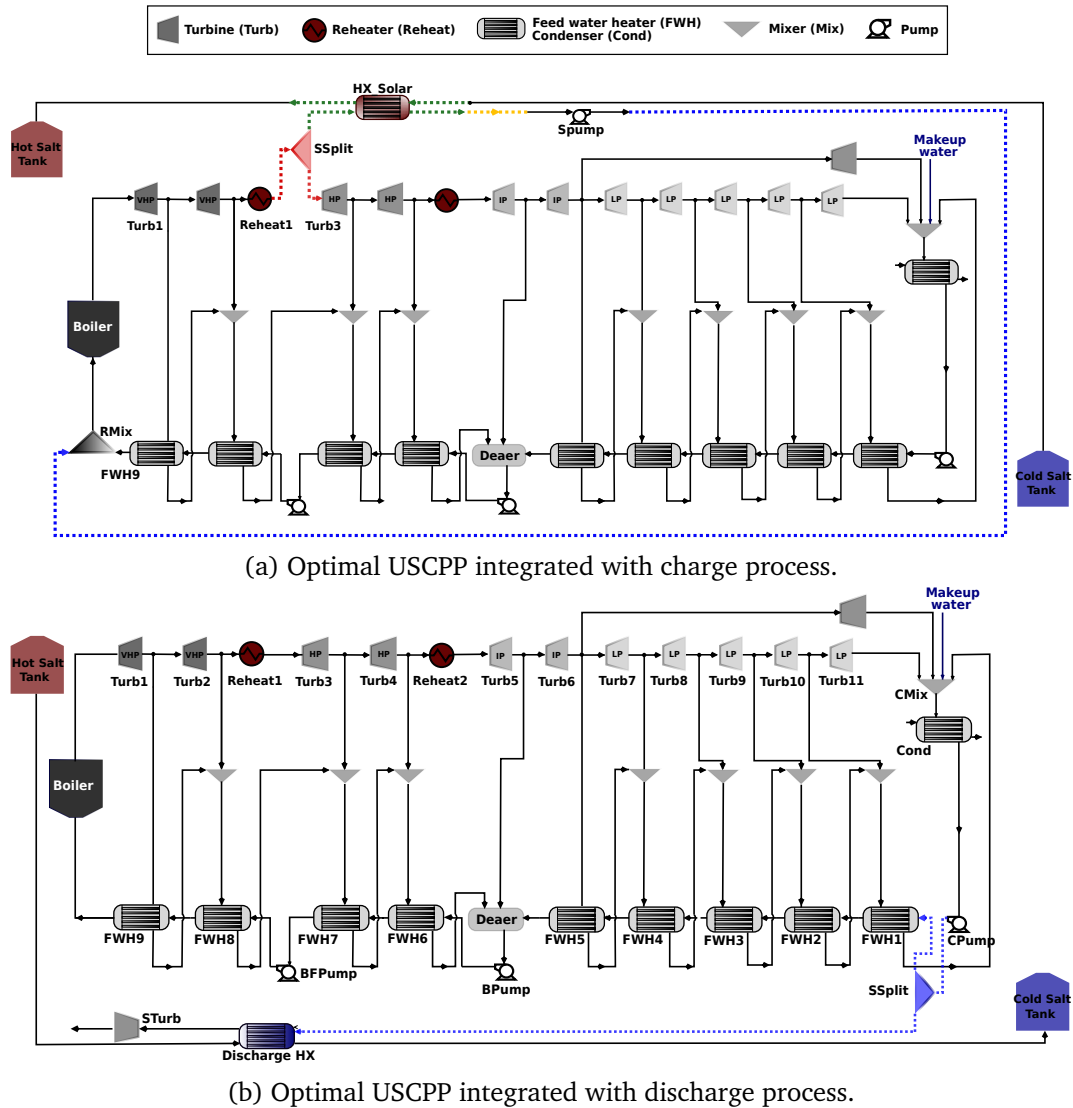


Figure 6: Optimal process flowsheet for ultra-supercritical plant (USCPP) integrated with (a) charge and (b) discharge TES after the solution of the GDP superstructures in Step 1.

Summary and Discussion

From all the feasible configurations for the charge and discharge USCPP superstructures in Tables 5 and 6, we observe that with the use of GDP we are able to explore multiple solution alternatives and some with similar objective values, allowing the user to select a configuration that adapts better to the conditions of the thermal cycle. This flexibility to select from multiple optimal designs opens the possibility of multiple power plant configurations that can integrate TES into their thermal cycles without affecting their thermal performance. We were able to enumerate the entire set of configurations for each superstructure using the RIC strategy in the solver GDPopt. The charge

superstructure problem solves in about 2,293 seconds when exploring the 60 configurations while the discharge superstructure solves in about 77 seconds when exploring the 11 configurations.

3.2 Step 2: Multi-period Optimization Under Price-taker Assumption

We formulated a multi-period optimization problem using the integrated USCPP model to study and design the TES under time-varying electricity prices. The multi-period optimization model includes an integrated USCPP model for each time period, where the integrated USCPP model is constructed using the optimal discrete decisions obtained from the solution of the design problem solved in Step 1. Figure 7 shows the integrated USCPP including both charge and discharge processes within the USCPP. Table 7 shows the optimization results for the multi-period optimization under the price-taker assumption considering two different cases: (i) operation-only and (ii) simultaneous design and operation. Both cases are solved for an average-day and average-week (See 2.2). In the operation-only case, the continuous design variables including charge and discharge heat exchanger areas, temperature of hot storage material, and amount of storage material are fixed to the values obtained during the design stage or Step 1 (i.e., rank 1 feasible design in Tables 5 and 6). The operation-only case evaluates the operation of a TES that was designed without considering time-varying electricity prices in a market under the price-taker assumption. In the simultaneous design and operation case, the design variables are optimized while considering time-varying electricity prices for the representative periods. The design obtained from the solution of the simultaneous case is then compared against the operation-only case.

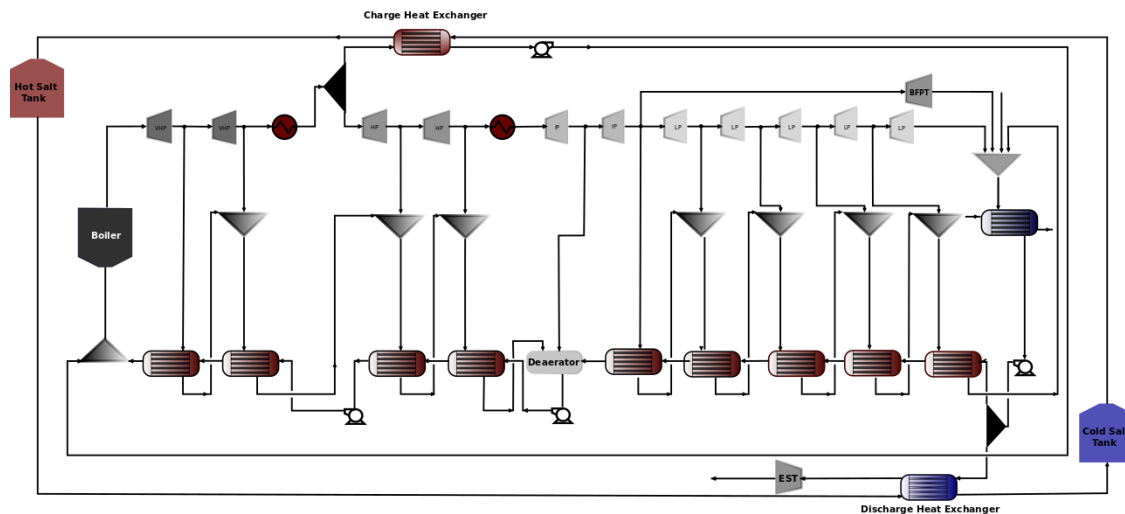


Figure 7: Process flowsheet of optimal integrated ultra-supercritical power plant with charge and discharge cycles at the optimal points of integration found during GDP design Step 1.

Analysis of Design Results

The results show that the simultaneous case is more efficient in designing a TES system as it can use the changes in the electricity prices to determine the optimal size of the TES. Table 7 shows that the simultaneous case yields a higher profit as compared to the operation-only case, i.e., \$1,729

vs. \$714 per day for the average-day scenario and \$2,367 vs. \$860 per day for the average-week scenario. The main reasons for the increased profits for the simultaneous case are as follows:

Lower capital costs. A smaller size and capacity of TES is obtained in the simultaneous case where the optimal design is determined considering time-varying electricity prices. This results in a lower capital cost, i.e., the costs for heat exchangers, storage material inventory, and storage tanks, of \$395 per day when using the average-day worth of electricity prices (or \$401 per day, when using the average-week worth of hourly prices) for the simultaneous case as compared to \$676 per day for the operation-only case. One reason for the lower capital cost is the need for a lower amount of storage material (i.e. Solar salt) in the simultaneous case, i.e. 3,111 tonnes when using the average-day price data (or 3,173 tonnes when using the average-week of hourly price data) vs. 6,841 tonnes. Also, the simultaneous case obtains a smaller charge heat exchanger area of about 1,531 m² and 1,562 m² for average-day and average-week, respectively as compared to 1,890.12 m² for the operation-only case. The oversizing of the TES design in the operation-only case is due to the potential of a fixed revenue arising from the assumption of a fixed average electricity price, i.e., \$22 and \$40 per MWh during charge and discharge design, respectively.

Higher revenue. The simultaneous case resulted in a 1% increase in the revenue, i.e., \$200,261 vs. \$198,030 for the average-day and \$203,397 vs. \$197,945 for the average-week because the total power generation increased by 0.8% (9,345 MW as compared to 9,273 MW). Table 7 shows that a main reason for the increase in revenue is the increase in the maximum operating temperature of the storage material, which increased to 853.15 K for the simultaneous case as compared to 826.56 K for the operation-only case. This increase in the operating temperature range for Solar salt makes available a higher specific enthalpy for the same amount of salt that can be used to generate additional power from the storage turbines.

Table 7: Results for the operation-only and simultaneous design and operation of the integrated ultra-supercritical power plant for the average-day and average-week. The variables marked with an * are variables that have a fixed value during the optimization.

Variable	Average-day		Average-week	
	Operation	Design and Operation	Operation	Design and Operation
Objective (\$/day)	713.91	1,729.15	860.21	2,366.94
Revenue (\$/day)	198,029.57	200,260.72	197,945.20	203,397.18
Capital Cost (\$/day)	675.76	394.96	675.76	401.43
Salt amount (metric tonnes)	6,840.52	3,111.14	6,840.52	3,173.10
Charge				
Heat exchanger area (m ²)	1,890.12*	1,531.03	1,890.12*	1,562.39
Hot salt temperature (K)	826.56*	853.15	826.56*	853.15
Salt flow to storage (kg/s)	Figure 8a	Figure 8c	Figure 8b	Figure 8d
Discharge				
Heat exchanger area (m ²)	436.44*	674.15	436.44*	674.15
Hot salt temperature (K)	826.56*	853.15	826.56*	853.15
Salt flow to storage (kg/s)	Figure 8a	Figure 8c	Figure 8b	Figure 8d

Figure 8 further shows that the design obtained in the simultaneous case is better than the one used in the operation-only case in terms of storage utilization. The maximum storage utilization (i.e., $TES^{utilization}$) of the available salt inventory is computed as $TES^{utilization} = \left(\frac{I^{max,hot}}{I^{total}} \right) \cdot 100$.

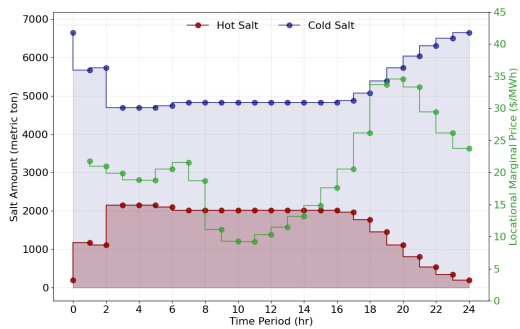
Figures 8a and 8c show the maximum storage utilization to be about 89% for the simultaneous case as compared to around 32% for the operation-only case. The lower utilization of storage inventory in the operation-only case is due to oversizing the TES. This can be further illustrated from the analysis of the storage operating profiles in Figures 8a and 8c, where the electricity prices π are shown as the green lines, while the red and blue shaded areas represent the amount of hot and cold salt at the end of each time period in the storage tanks, respectively. Note that for each and all cases, the initial and final states of storage tanks are the same (Equation 4k). As seen from Figure 8, the electricity prices are higher than \$26 per MWh during hours 18 and 24 in the average-day, while they are lower than \$22 per MWh from hours 0 to 18. This presents a clear incentive for the integrated generator and storage plant to store energy when the electricity prices are relatively lower (i.e., from hours 0 to 18) and then use the stored energy to produce power when the electricity prices are high (i.e., from hours 18 to 24). Evidently, the storage follows this intuitive approach and charges storage by building up the inventory for the hot salt (red shaded areas in Figure 8) from hours 0 to 18 and then discharges the storage from hours 18 to 24. Specifically, Figures 8a and 8c show similar trends, where the storage is charged initially and then discharged monotonously from hours 18 to 24. The difference, however, between these is in the maximum utilization. It is interesting to note that for both cases, the storage discharge profiles from hours 18 to 24 look the same. However, the storage charge profiles from 0 to 17 hours are slightly different; in the operation-only case the storage charges at a higher rate from hours 0 to 2, and then the plant is turned down to its minimum power capacity, whereas in the simultaneous case, the plant continues to operate at a capacity higher than its minimum and thus at a higher efficiency while charging the storage from hours 0 to 17. Both approaches result in similar operating costs for the integrated USCPP.

Effect of Time Horizon

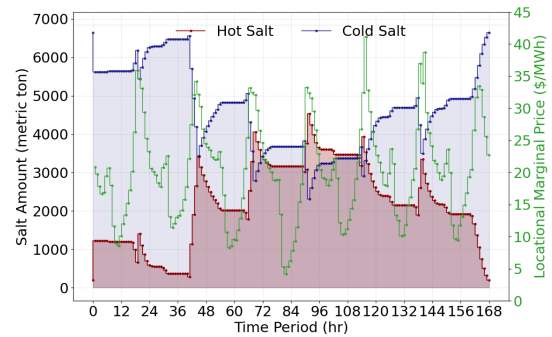
In this section, we study the effect of using a longer time horizon, e.g., a week as compared to a day, on the design of the TES. For this, we use the electricity prices for the average-week and solve the simultaneous case design model considering electricity prices for each day of the average-week, i.e., seven 24-hour time periods. We then compare the seven designs of TES obtained for each day of the average-week with the TES design obtained from solving the simultaneous model for the entire average-week. The primary difference between them is in how the periodic constraint, i.e., Equation 4k, is enforced. In the scenario where each day of the average-week is considered, the periodic constraint is enforced at the end of each day (or 24-hour time period), while for the average-week the periodic constraint (Equation 4k) is enforced only at the end of the week, thus allowing TES to consider daily variations in electricity prices.

The results in Table 7 show that the overall profit is improved by 19 % to \$2,367 per day when the design model was solved considering the entire average-week as compared to the average profit for all seven days when solved separately, i.e., \$1,924 per day. Table 8 shows the designs obtained from each of the seven problems, where the overall profit is in the range of \$-13,977 to \$6,207 per day, the charge heat exchanger area is in the range of 1,380 to 1,609 m², and the amount of salt required varies from 2,883 to 3,287 metric tonnes. The design of the TES obtained from considering the entire average-week of electricity prices in the same problem is within this range, where the total inventory of salt is 3,111 metric tonnes and the charge heat exchanger area is 1,531.03 m². This analysis highlights the need for including longer time horizons in the design analysis for designing long-term storage, where not only daily but weekly and seasonal price variations can be used for

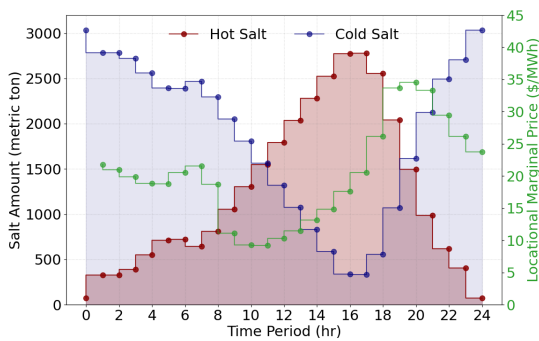
designing the TES.



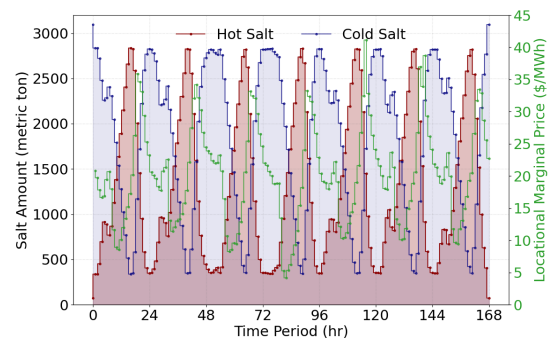
(a) Salt profiles for operation-only analysis for the average-day.



(b) Salt profiles for operation-only analysis for the average-week.



(c) Salt profiles for simultaneous design and operation analysis for the average-day.



(d) Salt profiles for simultaneous design and operation for the average-week.

Figure 8: Optimal profiles for the hot and cold salt amount for the (a) operation-only average-day, (b) operation-only average-week, (c) simultaneous design and operation for the average-day, and (d) simultaneous design and operation for the average-week.

Table 8: Results for the individual days in the average-week time horizon for the simultaneous case multi-period model.

Day	Profit (\$/day)	Variable		
		Area Heat Exchanger (m ²)		Amount of Salt (metric tonnes)
		Charge	Discharge	
1	-2,509.66	1,408.61	674.15	3,126.73
2	6,206.53	1,595.99	674.15	3,210.26
3	2,908.27	1,572.46	674.15	3,053.99
4	-13,977.10	1,379.86	674.15	2,892.95
5	5,919.28	1,563.06	674.15	3,287.17
6	10,597.14	1,597.40	674.15	3,097.80
7	4,325.60	1,609.35	674.15	2,883.36

4. Conclusions

In this work, we addressed two major challenges in the design and operation of integrated thermal energy systems while considering electricity markets: (i) use of detailed process-level models to determine the optimal integration of a thermal energy storage system (TES) with a thermal generator, and (ii) use of dynamic electricity prices to determine the optimal size and operation of a TES using a price-taker assumption. Specifically, in this study we presented a two-step approach for the simultaneous design and integration of a TES, highlighting the importance of optimization-based approaches for the conceptual design of integrated energy systems. The proposed workflow was successfully demonstrated using a case study involving a molten salt-based TES integrated with an ultra-supercritical power plant (USCPP). In Step 1, we used a Generalized Disjunctive Programming (GDP) based approach to solve two superstructure optimization problems (one for charge and one for discharge to integrate the TES system with the power plant) and determined the optimal discrete decisions for process-level integration of the TES with a thermal generator. In Step 2, we solved a multi-period optimization problem using time-varying electricity prices to obtain the optimal design of the TES including storage size, heat exchanger areas, and operating temperatures.

From Step 1, we obtained the best alternatives for integrating TES with USCPP during charge and discharge processes while also ranking other feasible designs in terms of their net profit. The analysis of the top seven solutions showed the effect of each discrete decision on net profit. For example, for the charge cycle superstructure, the analysis showed that the choice of storage material has a major impact on the overall cost followed by the choice of steam extraction point, whereas the choice of installing a cooler has the least impact on the net profit, which leads to multiple solutions with similar objectives in the set of ranked solutions. Similarly, for the discharge cycle superstructure, the analysis showed that the inlet pressure of the water to the TES has the most significant impact on the objective, whereas the alternative with intermediate pressure was more suitable for generating steam. From the solution of Step 2, i.e., the simultaneous design and operation problem, we obtained the optimal size of the TES for given electricity prices and time horizons. The comparison between the design obtained from Step 1 with the design obtained from Step 2 showed that the TES was over-designed when static or time-invariant electricity prices were considered. This is evident when observing the operational profile of TES, where the storage utilization is 89% for the simultaneous case, which uses time-varying electricity prices and is only 32% for the operations-only case, which uses time-invariant electricity prices. The results also show that the capital costs were reduced by nearly 40% when considering time-varying electricity prices. Further analysis showed that when considering longer time horizons for electricity prices, e.g., average-week, the design model was able to capture day-to-day variations in the electricity prices to design a TES system that improved the overall profit by 19%. These results highlight the need for using longer time horizons for price signals to capture seasonal changes in the electricity market.

In this work, the use of detailed process-level nonlinear models with rigorous property calculations limited the study to consider moderate-size time horizons of up to one week. In the near future, we will explore the use of surrogate models to replace these detailed process models, which will enable the use of longer time horizons with our proposed workflow. Such an analysis will allow us to capture seasonal price variability in the TES design and optimization problem. In addition, historical data for electricity prices for a given market can be used instead of the generic RTS-GMLC dataset used in our design problem. This use of historical data will allow us to determine a design of an IES that better fits the desired market. We also look to extend our study to go beyond the price-taker assumption by explicitly including market interactions of the IES by obtaining potential revenue models from a production cost model using a stochastic programming approach.

Finally, this case study demonstrates the use of DISPATCHES and IDAES[®] open-source platforms for the construction of first-principle models using an equation-oriented modeling framework and rigorous property calculations, dynamic market analysis capabilities through grid-integration tools, and advanced optimization capabilities. This workflow can be easily applied to TES systems beyond molten-salt and oil-based and to other energy systems such as NGCC with CO₂ capture, biomass gasification for co-producing hydrogen and electricity with CO₂ capture, nuclear power generators with TES, and concentrated solar power with TES.

A. Ultra-supercritical Power Plant and Storage System Models

In Table 9, we include all the unit models used for the construction of the ultra-supercritical power plant model (USCPP) and the thermal energy storage system (TES) with their main assumptions, while the property packages used in the units are given in Table 10.

Table 9: IDAES[®] unit models used for the construction of the ultra-supercritical power plant model.

Unit Operation	IDAES [®] Unit Model	Main Assumptions
Turbine	HelmTurbineStage	Isentropic
Feed water heater	HeatExchanger	Underwood Assumption
Pump	HelmIsentropicCompressor	Isentropic
Mixer	HelmMixer	Minimum Pressure
Splitter	HelmSplitter	Isenthalpy
Boiler, Reheaters	Heater	

Table 10: DISPATCHES and IDAES[®] property packages used in the ultra-supercritical power plant model integrated with storage system.

Property Package	Properties
Solar salt [15]	60% NaNO ₃ and 40% KNO ₃ Temperature range (K): [513.15, 853.15]
Hitec salt [34, 8]	40% NaNO ₂ , 7% NaNO ₃ , and 53% KNO ₃ Temperature range (K): [435.15, 788.15]
Thermal oil [14]	Therminol-66 Temperature range (K): [260, 616]

B. Data for Ultra-supercritical Power Plant Model

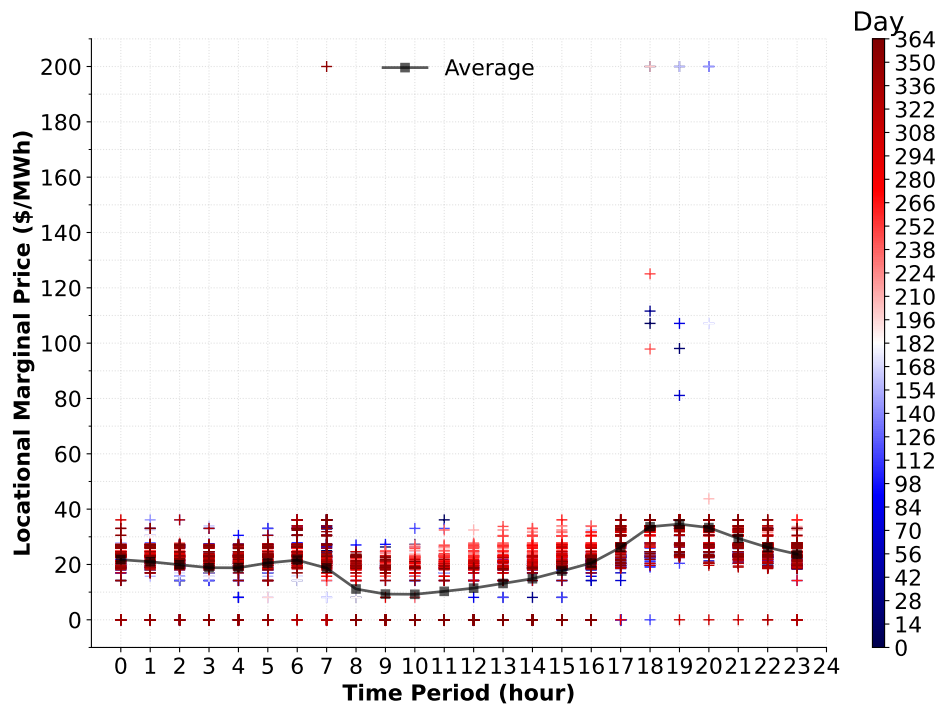
In Table 11, we include all the operational and parameters assumed for various unit operations in the ultra-supercritical power plant model, such as pressure ratio and isentropic efficiency for all turbines, the area and overall heat transfer coefficient (*OHTC*) for feed water heaters, and pressure change and isentropic efficiency for all pumps. The assumed values for the parameters are to match the performance of the simplified power plant model to the available data in Department of Energy technical report DOE/FE-0400 [11].

Table 11: Data for the ultra-supercritical power plant model.

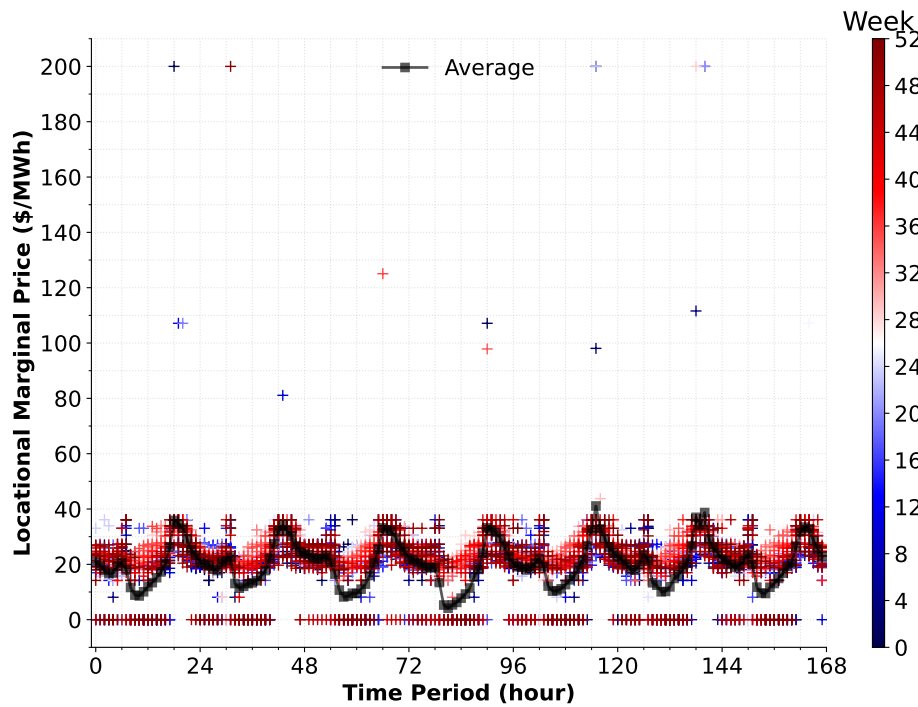
IDAES [®] Unit	Variable	Value
Turbine 1, 2, 3, 4	Pressure ratio	0.388, 0.774, 0.498, 0.609
	Isentropic efficiency	0.940
Turbine 5, 6	Pressure ratio	0.523, 0.495
	Isentropic efficiency	0.880
Turbine 7, 8, 9, 10, 11	Pressure ratio	0.514, 0.389, 0.572, 0.476, 0.204
	Isentropic efficiency	0.740
Feed Water Heater 1, 2, 3, 4, 5, 6, 7, 8, 9	Area (m ²)	250, 195, 164, 208, 152, 207, 202, 215, 175
	OHTC (W/m ² /K)	3000
Condenser Pump	Delta pressure (Pa)	2313881
	Isentropic efficiency	0.800
Booster Pump	Delta pressure (Pa)	5715067
	Isentropic efficiency	0.800
Boiler Feedwater Pump	Isentropic efficiency	0.8

C. Average RTS-GMLC Data

Since the integrated model used in the multi-period model formulation involves a large number of nonlinear constraints and variables, we calculate the average price of electricity at each hour for a representative day and week of the year using the RTS-GMLC data set in Section 2.2 in Figure 1. Figure 9a shows the average values with a black line for the representative day or average-day (24-hour time period) while the data for the π for the 364 days for each hour is plotted using the "+" marker with different colors for each day as given in the color bar on the right of the plot. For the representative week or average-week (168-hour time period) of the year, we organize the data in 168-hour time horizons and calculate the average value of the π for each respective hour. Figure 9b shows the average values for the average-week as a black line, and the RTS-GMLC data for each day of the year is plotted using the plus "+" marker.



(a) Average-day or 24-hour time horizon.

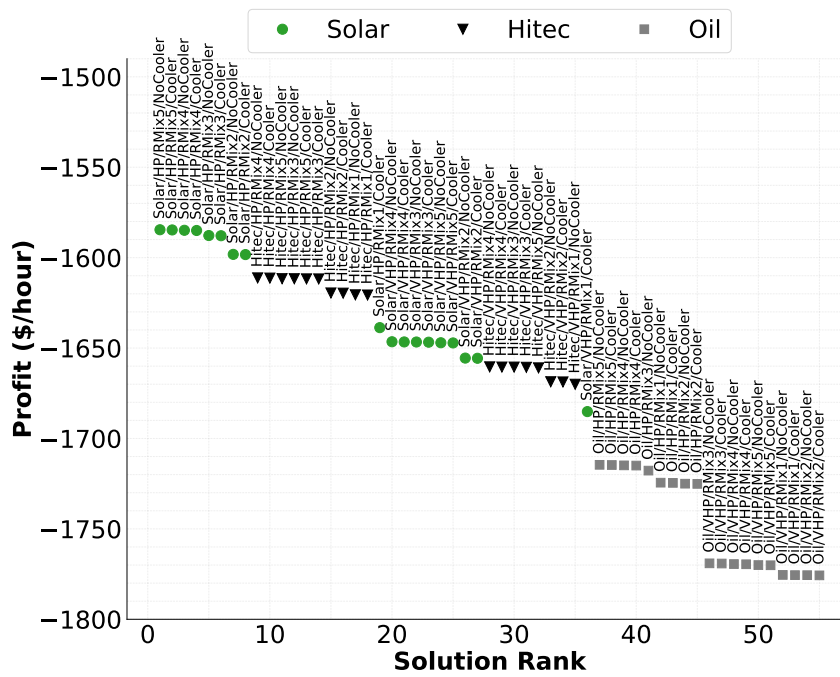


(b) Average-week or 168-hour time horizon.

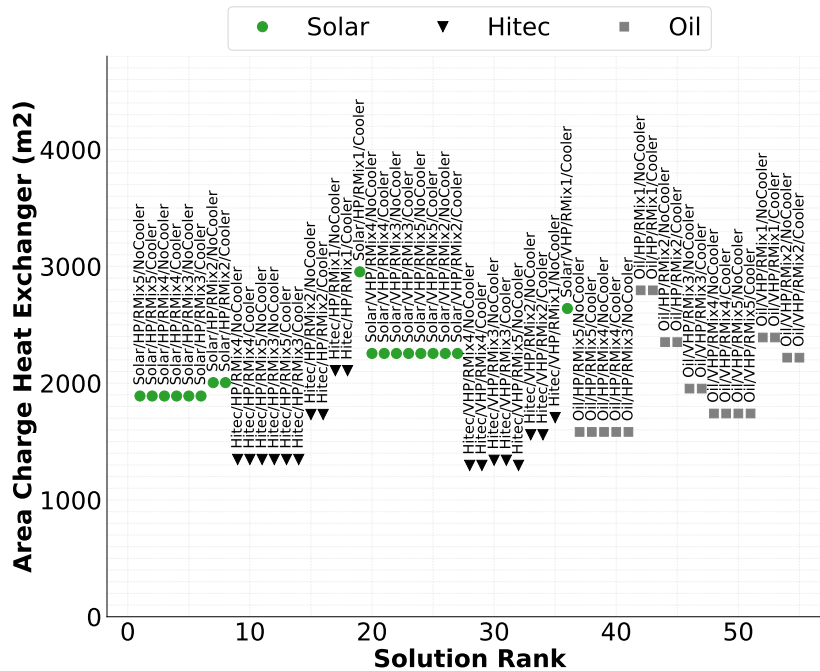
Figure 9: RTS-GMLC dataset for the average-day and average-week of the year.

D. GDP Superstructures Feasible Designs

Figures 10 and 11 show all the feasible designs explored by the solver GDPopt for the charge and discharge superstructures.

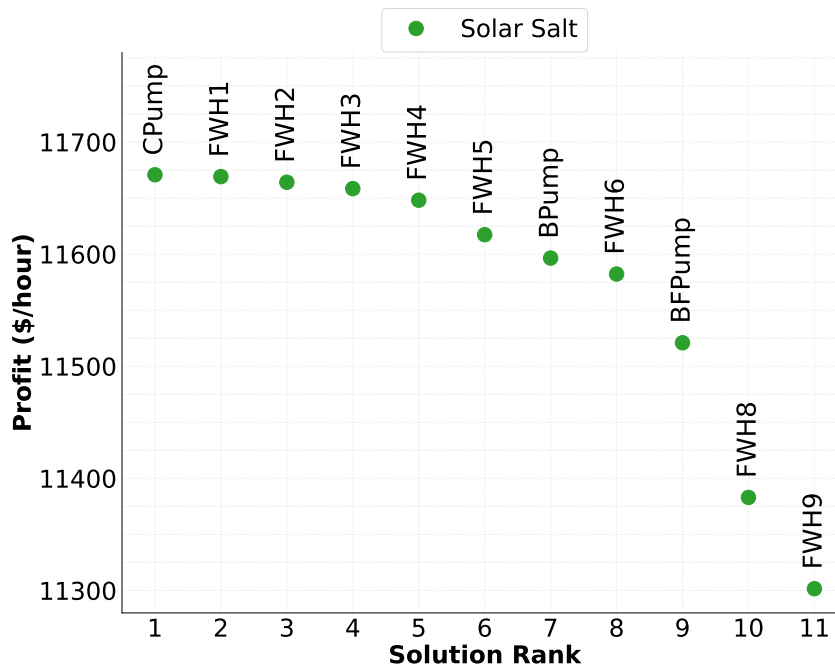


(a) Profit results for all feasible designs.

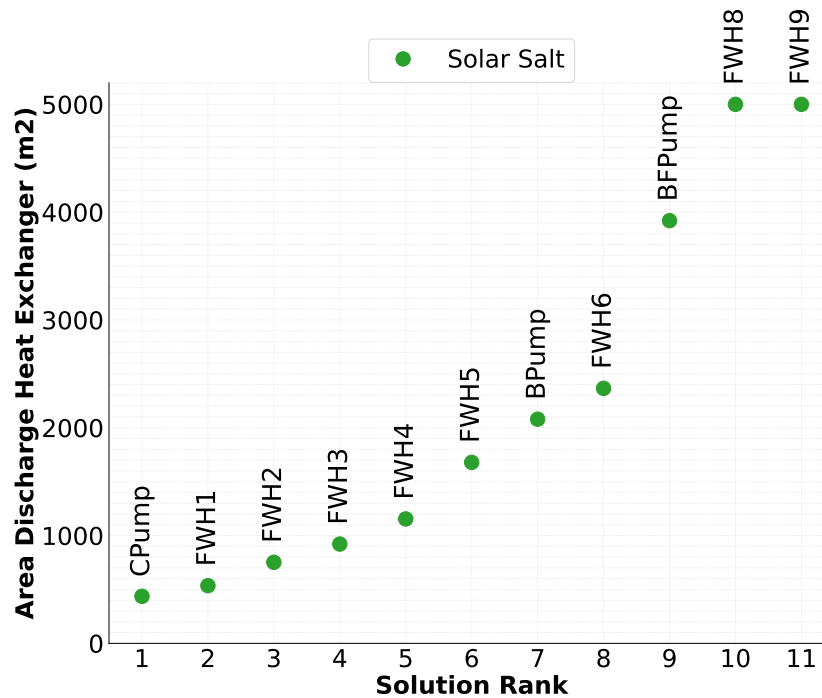


(b) Area of charge heat exchanger results for all feasible designs.

Figure 10: Results for the (a) profit (a) and (b) area of charge heat exchanger for all feasible designs identified during the solution of the discrete design decisions of the charge USCPP superstructure. The feasible designs correspond to 55 of the 60 explored configurations.



(a) Profit results for all feasible designs.



(b) Area of discharge heat exchanger results for all feasible designs.

Figure 11: Results for the (a) profit and (b) area of discharge heat exchanger for all feasible designs identified during the solution of the discrete design decisions of the discharge USCPP superstructure.

Abbreviations and Nomenclature

Abbreviations

BFPump Boiler feed pump unit equipment

Boiler Boiler or heater unit equipment

BPump Booster pump unit equipment

CMix Condenser mixer unit equipment

CPump Condenser pump unit equipment

CSP Concentrated Solar Power

Deaer Deaerator unit equipment

DISPATCHES Design Integration and Synthesis Platform to Advance Tightly Coupled Hybrid Energy Systems

FWH Feed water heater

GDP Generalized Disjunctive Programming

HP High pressure

HX Heat exchanger unit equipment

IDAES Institute for the Design of Advanced Energy Systems

IES Hybrid energy system

IP Intermediate pressure

LP Low pressure

MINLP Mixed-integer Nonlinear Programming

NGCC Natural gas combined cycle

Reheat Reheater unit equipment

RMix Recycle mixer unit equipment

RTS Reliability Test System
SPump Storage pump unit equipment
STurb Storage turbine unit equipment
TES Thermal energy storage
Turb Turbine unit equipment
USCPP Ultra-supercritical power plant
VHP Very high pressure

Sets

\mathcal{K} Set of disjuncts or alternatives in GDP formulation
 \mathcal{S} Set of storage materials
 \mathcal{T} Set of time periods
 \mathcal{X} Set of variables
 \mathcal{Z} Set of disjunctions

Variables

$CAPEX$ Annualized capital cost in \$/year
 d Design variables
 d^c Continuous design decisions
 d^d Discrete design decisions
 F Flow in mol/s
 I Inventory of storage material in mass units
 N Nonanticipativity variable
 $OHTC$ Overall Heat Transfer Coefficient in W/m²/K
 $OPEX$ Operating costs in \$/hour
 p Pressure in Pa
 P Power plant power in MW
 REV Revenue in \$/hour
 x Variables in the system
 Y State variables: flow, pressure, and enthalpy

Parameters

C Cost in \$/hour

π Locational marginal price in \$/kWh

ρ Ramp rate of power plant in MW

Superscripts

average Superscript to indicate an average value

charge Superscript to indicate a charge cycle stream

coal Superscript to indicate a coal stream

discharge Superscript to indicate a discharge cycle stream

hot Superscript to indicate a hot stream

lb Superscript to indicate lower bound

smaterial Superscript to indicate a storage material stream

total Superscript to indicate total value of variable

ub Superscript to indicate upper bound

Subscripts

cold Superscript to indicate a cold stream

Hitec Subscript to indicate Hitec salt as the storage material

in Subscript to indicate an inlet in a stream

oil Subscript to indicate Thermal oil salt as the storage material

out Subscript to indicate an outlet in a stream

Solar Subscript to indicate Solar salt as the storage material

Bibliography

- [1] I. E. Agency. Electricity market report. Technical report, International Energy Agency, Paris, 2020.
- [2] G. Alva, Y. Lin, and G. Fang. An overview of thermal energy storage systems. *Energy*, 144:341–378, 2018.
- [3] C. Barrows, A. Bloom, A. Ehlen, J. Ikäheimo, J. Jorgenson, D. Krishnamurthy, J. Lau, B. McBennett, M. O’Connell, E. Preston, A. Staid, G. Stephen, and J.-P. Watson. The IEEE reliability test system: A proposed 2019 update. *IEEE Transactions on Power Systems*, 35(1):119–127, 2020.
- [4] M. Barttfeld, P. A. Aguirre, and I. Grossmann. Optimal synthesis of complex distillation columns using rigorous models. *Computers & Chemical Engineering*, 29:1203–1205, 2005.
- [5] M. Barttfeld, P. A. Aguirre, and I. E. Grossmann. Alternative representations and formulations for the economic optimization of multicomponent distillation columns. *Computers & Chemical Engineering*, 27(3):363–383, 2003.
- [6] K. Burnard and O. Ito. Technology roadmap: High-efficiency, low-emissions coal-fired power generation. Technical report, International Energy Agency, 2012.
- [7] M. L. Bynum, G. A. Hackebeil, W. E. Hart, C. D. Laird, B. L. Nicholson, J. D. Siirola, J.-P. Watson, and D. L. Woodruff. *Pyomo—optimization modeling in Python*, volume 67. Springer Science & Business Media, third edition, 2021.
- [8] Z. Chang, X. Li, C. Xu, C. Chang, and Z. Wang. The design and numerical study of a 2MWh molten salt thermocline tank. *Energy Procedia*, 69:779–789, 2015.
- [9] Q. Chen, E. S. Johnson, D. E. Bernal, R. Valentin, S. Kale, J. Bates, J. D. Siirola, and I. E. Grossmann. Pyomo.GDP: an ecosystem for logic based modeling and optimization development. *Optimization and Engineering*, 23:607–642, 2022.
- [10] Q. Chen, Y. Liu, G. Seastream, J. D. Siirola, and I. E. Grossmann. Pyosyn: A new framework for conceptual design modeling and optimization. *Computers & Chemical Engineering*, 153:107414, 2021.
- [11] Department of Energy. Market-based advance coal power systems. Technical Report DOE/FE-0400, Office of Fossil Energy, 1999.

- [12] A. W. Dowling, R. Kumar, and V. M. Zavala. A multi-scale optimization framework for electricity market participation. *Applied Energy*, 190:147–164, 2017.
- [13] A. W. Dowling, T. Zheng, and V. M. Zavala. A decomposition algorithm for simultaneous scheduling and control of CSP systems. *AIChE Journal*, 64:2408–2417, 2018.
- [14] Eastman. Therminol 66, high performance highly stable heat transfer fluid (0c to 345c), 2019.
- [15] R. Ferri, A. Cammi, and D. Mazzei. Molten salt mixture properties in RELAP5 code for thermodynamic solar applications. *International Journal of Thermal Sciences*, 47(12):1676–1687, 2008.
- [16] L. F. Fuentes-Cortés, A. W. Dowling, C. Rubio-Maya, V. M. Zavala, and J. M. Ponce-Ortega. Integrated design and control of multigeneration systems for building complexes. *Energy*, 116:1403–1416, 2016.
- [17] X. Gao, B. Knueven, J. D. Sirola, D. C. Miller, and A. W. Dowling. Multiscale simulation of integrated energy system and electricity market interactions. *Applied Energy*, 316:119017, 2022.
- [18] O. Garbrecht, M. Bieber, and R. Kneer. Increasing fossil power plant flexibility by integrating molten-salt thermal storage. *Energy*, 118:876–883, 2017.
- [19] J. H. Ghose, Q. Chen, M. A. Zamarripa, A. Lee, A. P. Burgard, I. E. Grossmann, and D. C. Miller. A comparative study between GDP and NLP formulation for conceptual design of distillation columns. *Computers & Chemical Engineering*, 44:865–870, 2018.
- [20] C. Grigg, P. Wong, P. Albrecht, R. Allan, M. Bhavaraju, R. Billinton, Q. Chen, C. Fong, S. Haddad, S. Kuruganty, W. Li, R. Mukerji, D. Patton, N. Rau, D. Reppen, A. Schneider, M. Shahidehpour, and C. Singh. The IEEE reliability test system-1996. a report prepared by the reliability test system task force of the application of probability methods subcommittee. *IEEE Transactions on Power Systems*, 14(3):1010–1020, 1999.
- [21] L. Gurobi Optimization. Gurobi optimizer reference manual, 2023.
- [22] IEA Clean Coal Centre. Increasing the flexibility of coal-fired power plants. Technical report, IEA, 2016.
- [23] J. R. Jackson and I. Grossmann. A disjunctive programming approach for the optimal design of reactive distillation columns. *Computers & Chemical Engineering*, 25:1661–1673, 2001.
- [24] J. Javaloyes-Antón, R. Ruiz-Femenia, and J. A. Caballero. Rigorous design of complex distillation columns using process simulators and the particle swarm optimization algorithm. *Industrial & Engineering Chemistry Research*, 52(44):15621–15634, 2013.
- [25] M. Krugger, S. Muslubas, T. Loeper, F. Klasing, P. Knodler, and C. Mielke. Potentials of thermal energy storage integrated into steam power plants. *Energies*, 13:2226, 2020.
- [26] A. Lee, J. H. Ghose, J. C. Eslick, C. d. Laird, J. D. Sirola, M. A. Zamarripa, D. Gunter, J. H. Shinn, A. W. Dowling, D. Bhattacharyya, L. T. Biegler, A. P. Burgard, and D. C. Miller. The IDAES process modeling framework and model library - flexibility for process simulation and optimization. *Journal of Advanced Manufacturing and Processing*, 3:1–30, 2021.

- [27] D. Li and J. Wang. Study of supercritical power plant integration with high temperature thermal energy storage for flexible operation. *Journal of Energy Storage*, 20:140–152, 2018.
- [28] J. Ma, M. A. Zamarripa, J. C. Eslick, Q. M. Le, D. Bhattacharyya, L. T. Biegler, S. E. Zitney, A. P. Burgard, and D. C. Miller. Dynamic simulation and optimization of a subcritical coal-fired power plant during load-ramping operations. In Y. Yamashita and M. Kano, editors, *14th International Symposium on Process Systems Engineering*, volume 49 of *Computer Aided Chemical Engineering*, pages 1033–1038. Elsevier, 2022.
- [29] J. Martinek, J. Jorgenson, M. Mehos, and P. Denholm. A comparison of price-taker and production cost models for determining system value, revenue, and scheduling of concentrating solar power plants. *Applied Energy*, 231:854–865, 2018.
- [30] L. Mencarelli, Q. Chen, A. Pagot, and I. E. Grossmann. A review on superstructure optimization approaches in process system engineering. *Computers & Chemical Engineering*, 136:106808, 2020.
- [31] E. S. Rawlings, Q. Chen, I. Grossmann, and J. A. Caballero. Kaibel column: Modeling, optimization, and conceptual design of multi-product dividing walls. *Computers & Chemical Engineering*, 125:31–39, 2019.
- [32] W. D. Seider, D. R. Lewin, J. Seader, and S. Widagdo. *Product and Process Design Principles: Synthesis Analysis and Evaluation*. John Wiley & Sons, Inc., third edition, 2009.
- [33] R. Sioshansi and P. Denholm. The value of concentrating solar power and thermal energy storage. *IEEE Transactions on Sustainable Energy*, 1(3):173–183, 2010.
- [34] M. S. Sohal, M. A. Ebner, P. Sabharwall, and P. Sharpe. Engineering database of liquid salt thermophysical and thermochemical properties. Technical report, Idaho National Laboratory, 2013.
- [35] M. Sun, T. Liu, X. Wang, T. Liu, M. Li, G. Chen, and D. Jiang. Roles of thermal energy storage technology for carbon neutrality. *Carbon Neutrality*, 2:12, 2023.
- [36] F. Trespalacios and I. E. Grossmann. Review of mixed-integer nonlinear and generalized disjunctive programming methods. *Chemie Ingenieur Technik*, 86:991–1012, 2014.
- [37] A. Wächter and L. T. Biegler. On the implementation of a primal-dual interior point filter line search algorithm for large-scale nonlinear programming. *Mathematical Programming*, 106:25–57, 2006.
- [38] J. D. Wojcik and J. Wang. Technical feasibility study of thermal energy storage integration into the conventional power plant cycle. *Energies*, 10:1–19, 2017.
- [39] H. Yeomans and I. E. Grossmann. A systematic modeling framework of superstructure optimization in process synthesis. *Computers & Chemical Engineering*, 23(6):709–731, 1999.
- [40] H. Yeomans and I. E. Grossmann. Disjunctive programming models for the optimal design of distillation columns and separation sequences. *Industrial & Engineering Chemistry Research*, 39:1637–1648, 2000.
- [41] Q. Yong, Y. Tian, X. Qian, and X. Li. Retrofitting coal-fired power plants for grid energy storage by coupling with thermal energy storage. *Applied Thermal Engineering*, 215:119048, 2022.

- [42] K. Zhang, M. Liu, Y. Zhao, H. Yan, and J. Yan. Design and performance evaluation of a new thermal energy storage system integrated within a coal-fired power plant. *Journal of Energy Storage*, 50:104335, 2022.